Dynamics of former ice lobes of the southernmost Patagonian Ice Sheet based on a glacial landsystems approach

---

Christopher M. Darvill*[1,†], Chris R. Stokes[1], Michael J. Bentley[1], David, J. A. Evans[1] & Harold Lovell[2]

*E-mail: christopher.darvill@unbc.ca

[1] Department of Geography, Durham University, South Road, Durham, DH1 3LE, UK.

[2] Department of Geography, University of Portsmouth, Portsmouth, UK.

† Present address: Geography Program and Natural Resources and Environmental Studies Institute, University of Northern British Columbia, 3333 University Way, Prince George, BC, V2N 4Z9, Canada.

Abstract

Reconstructions of former ice masses from glacial geomorphology help constrain the nature and timing of glaciation in relation to climatic forcing. This paper presents a new reconstruction of the glacial history of five ice lobes in southernmost South America: the Bahía Inútil – San Sebastián, Magellan, Otway, Skyring, and Río Gallegos ice lobes. We use previous geomorphological mapping of glacial landforms to reconstruct former glacial limits and proglacial lakes, demarcate flow-sets from the distribution of glacial lineations, and evaluate glacial landsystem signatures and their palaeoglaciological implications. Evidence suggests that the ice lobes predominantly reflect active temperate glacial landsystems, which may have switched to polythermal systems when periods of cold-based ice developed ephemerally. This complex landsystem signature implies that the ice lobes were sensitive to regional climate variability, with active re-advances during overall retreat of the ice margins. There is also evidence for periods of fast ice flow and possible surge-like activity in the region, followed by the rapid retreat or even collapse of some of the ice lobes in association with proglacial lakes. Constraining our new reconstruction with published chronological information suggests that at least some of the ice lobes advanced prior to the global Last Glacial Maximum (gLGM: *ca*. 26.5-19 ka) during the last glacial cycle. Our new reconstruction demonstrates a more complex picture of ice dynamics than has previously been portrayed, and one in which the advance and retreat of the ice lobes was likely to have been primarily driven by changes in climate. As such, ice advances prior to the gLGM in the southernmost part of the Patagonian Ice Sheet are likely to be indicative of a wider climatic forcing at this time.

1 Introduction

Well-preserved glacial geomorphology relating to the former Patagonian Ice Sheet provides a record of the fluctuations of its margins throughout the Quaternary (Clapperton, 1993; Glasser & Jansson, 2008; Glasser et al., 2008). This record can also be used to reconstruct ice-sheet dynamics (Glasser & Jansson, 2005; Glasser et al., 2005; Lovell et al., 2012) and may be supplemented with chronological information to constrain how the ice sheet changed over time as a result of climatic forcing (e.g. McCulloch et al., 2005b; Douglass et al., 2006; Kaplan et al., 2008a, 2008b; Hein et al., 2010). For example, the southernmost part of the ice sheet was heavily influenced by changes in temperature and precipitation linked to the atmospheric Southern Westerly Winds and oceanic frontal positions (Lamy et al., 2007; Kaplan et al., 2008a; Kilian & Lamy, 2012). Climate reconstructions prior to the Holocene are uncertain, but temperatures at the global Last Glacial Maximum (gLGM: *ca*. 26.5-19 ka, Clark et al., 2009) may have been as much as 7-8ºC lower than present (Benn & Clapperton, 2000a; Caniupán et al., 2011). Consequently, reconstruction of the southernmost ice lobes can help to establish likely changes in these climatic systems over time, but this process requires a robust understanding of the glacial history and ice dynamics (Sugden et al., 2005; Kilian & Lamy, 2012).

Previous studies of the southernmost ice lobes of the Patagonian Ice Sheet have tended to focus on dating glacial limits, with a particular emphasis on constraining the local Last Glacial Maximum in relation to the gLGM and younger glacial limits. However, there has been a lack of consistent, detailed mapping across the region (Darvill et al., 2014), and there remains uncertainty about the timing and nature of pre-gLGM glacial advances (Kaplan et al., 2007). Indeed, it has been shown that glacial limits of the Bahía Inútil – San Sebastián (BI-SSb) ice lobe that were previously thought to be pre-last glacial cycle were actually deposited more recently (Darvill et al., 2015b). This suggests that significant glacier advances during Marine Isotope Stage (MIS) 3 (and possibly MIS 4) are represented in the area, perhaps linked to wider glacial activity in the southern mid-latitudes at this time

(Putnam et al., 2013; Kelley et al., 2014; Darvill et al., 2015b; Doughty et al., 2015; Schaefer et al., 2015; Eaves et al., 2016). In this paper, we use a previously published map of the region, largely based on relatively high-resolution satellite imagery (~30 m resolution; Darvill et al., 2014), and apply glacial inversion methods to produce a new palaeoglaciological reconstruction of the dynamics of the ice sheet that is further constrained through analysis of published chronological data.

2 Study area

The study area lies between 51-55°S and 68-73°W, and encompasses the area occupied by five former piedmont ice lobes of the Patagonian Ice Sheet (Figure 1). From south to north, these are the Bahía Inútil – San Sebastián (BI-SSb), Magellan, Otway, Skyring and Río Gallegos lobes. The topography of the area changes dramatically from southwest to northeast, with the southern Andes (dominated by the Cordillera Darwin) marking the southern and western boundaries and casting a strong rain shadow over the low, flat pampas and coastal areas to the north and east (Coronato et al., 2008). The locations of the former ice lobes are marked by prominent straits and sounds, which were established by one or more major glacial events during the Quaternary (Rabassa, 2008; Kaplan et al., 2009). Glacial geomorphology relating to the former ice lobes was first described in detail by Caldenius (1932) and has since been updated, and sometimes reinterpreted, by numerous workers (Clapperton et al., 1995; Rabassa et al., 2000; Benn & Clapperton, 2000b, 2000a; Meglioli, 1992; Bentley et al., 2005; McCulloch et al., 2005b; Lovell et al., 2011, 2012; Darvill et al., 2014, 2015a).

Meglioli (1992) used weathering indices to establish an age model for the region, whereby nested moraine limits were deposited during successive glacial episodes from MIS 12 to 2 (Coronato et al., 2004). Subsequently, a range of dating techniques have been used to constrain the ages of some moraine limits deposited during or after the gLGM (Rutter et al., 1989; Porter, 1990; Meglioli, 1992; Clapperton et al., 1995; McCulloch et al., 2005b; Sagredo et al., 2011; Blomdin et al., 2012; Hall et al., 2013). Age constraints prior to the gLGM are limited (Kaplan et al., 2007; Evenson et al., 2009; Darvill et al., 2015a, 2015b), although ^{40}Ar/^{39}Ar dates suggest that the outermost limits of the Río Gallegos, Skyring, Otway and Magellan lobes date to 1070-450 ka (Meglioli, 1992; Singer et al., 2004). By contrast, Darvill et al. (2015b) recently demonstrated that one of two outer limits of the BI-SSb lobe was deposited much more recently, at *ca*. 30 ka. Beyond this, the Magellan and Río Gallegos lobes have only a few scattered cosmogenic nuclide exposure ages (Kaplan et al., 2007; Evenson et al., 2009; Sagredo et al., 2011) and the Skyring and Otway lobes have no age controls prior to around 15 ka (Kilian et al., 2007, 2013).

Relatively little attention has been given to the nature of ice dynamics recorded by the glacial geomorphology, with the exception of localised studies on the gLGM or post-gLGM limits. Previous work has highlighted factors affecting ice-lobe dynamics and rates of advance and retreat, such as the influence of pro-glacial lakes (Porter et al., 1992; Lovell et al., 2012), subglacial thermal regime (Benn & Clapperton, 2000b, 2000a; Bentley et al., 2005) and evidence for rapid ice flow over a soft-sediment bed (Clapperton et al., 1995; Lovell et al., 2012). As such, there is a need for a regional glacial history that incorporates geomorphological evidence for ice dynamics and reassesses previously published chronological data.

3 Methods

3.1 Geomorphological mapping

This paper uses a previously-published glacial geomorphological map of the region (Darvill et al., 2014) to build a new palaeoglaciological reconstruction. Glacial landforms were mapped from Landsat and ASTER satellite images, aerial photographs, Google Earth imagery, and SRTM digital elevation data, and much of the area was also cross-checked in the field, with an emphasis on verifying mapped landforms and identifying cross-cutting relationships of features (Darvill et al., 2014).

3.2 Glacial flow-sets, ice margins and landsystems

Glacial landforms can yield information on the extent of former ice advances and ice sheet dynamics using glacial inversion methods (Kleman et al., 2006). Glacial lineation flow-sets reveal coherent patterns of former ice flow trajectories and a landsystem approach links assemblages of glacial geomorphological features to particular styles of glaciation (Evans, 2003a), many of which have modern analogues that aid the interpretation of former glacial and climatic conditions. Following Clark (1999), glacial lineations were grouped into flow-sets according to parallel concordance, close proximity and similar morphometry, as well as relationship to ice marginal features such as moraines and meltwater channels. By mapping glacial landforms systematically and comprehensively, we were able to both reconstruct glacial limits and assess landsystem types and their palaeoglaciological implications based on landform suites.

3.3 Proglacial lake reconstruction

The reconstruction of former proglacial lakes can yield information on the relative position of ice lobes and their dynamics. Following Stokes & Clark (2004) and Lovell et al. (2012), we modelled proglacial lake formation using a Digital Elevation Model (DEM), constructed from *ca*. 90 m resolution SRTM data for areas of land, and *ca*. 900 m resolution ETOPO data for submarine areas that may have been previously exposed. The DEM was filled in 10 m increments to examine where lakes developed and over-spilled in relation to former shorelines and ice margins. The DEM data is sufficient for a regional-scale assessment of where lakes were likely to have developed (*cf*. Lovell et al., 2012), but the coarser resolution of the ETOPO data means that over-spill channels beneath present sea-level may have been missed, and a lack of bathymetric data for present-day lakes means that their exact depths are unknown. Additionally, the DEM provides present-day land elevation and not that during glaciation, when the mass of the Patagonian Ice Sheet would have depressed the mountain range. This should be corrected for Glacio-Isostatic Adjustment (GIA), but the resolution of global model output, such as ICE-5G (Peltier, 2004), is too coarse to be of use for this purpose. Consequently, we reconstructed palaeolakes based on a contemporary DEM, but with the caution that they are likely minimum estimates of lake depth because the regional pattern of ice loading would have been to overdeepen slopes towards the west. The presence of lakes predicted by the DEM analysis was cross-checked and, although the field evidence is inherently fragmentary, we did not identify any obvious conflict between predicted lake levels and the presence of raised shorelines in the glacial geomorphological mapping.

4 Glacial Landform Assemblages

This section summarises the nature of the glacial landform assemblages in the study area. The results are in the form of a map published in Darvill et al. (2014) and we now describe and interpret the landform assemblages before discussing their palaeoglaciological significance in section 5.

4.1 Ice-marginal landforms

4.1.1 Moraine ridges

The clearest moraine ridges in the study area are those of the Skyring and Otway lobes, where numerous arcuate ridges are nested around the main depressions (Figure 2), marking the point at which the lobes were flowing up the adverse slopes of overdeepenings onto higher relief areas (Barr & Lovell, 2014). Similar moraines are found on the northern side of the Magellan lobe, particularly across Primera Angostura (Figure 2), within *ca*. 10 km of

Bahía Inútil in the BI-SSb lobe (Figure 3), and in the Río Gallegos lobe depression. Smaller, less distinctive ridges aligned perpendicular to former ice flow are often draped over other glacial features within the central Magellan and BI-SSb lobes, such as on Punta Gente, where ridges are draped over drumlinised terrain north of Porvenir (Bentley et al., 2005; Figure 4). Likewise, in the centre of the BI-SSb depression, ridges can be seen draped over both lineations and subdued moraine topography (Figure 3).

The ridges include terminal moraines (sharp-crested, arcuate ridges around the main depressions) and recessional moraines or recessional push moraines (smaller, less distinctive ridges perpendicular to ice flow and draping other features), although it is difficult to distinguish their form based on morphology alone. Two exceptions are where we have supplementary sedimentological evidence to support the landform data. A section through a moraine in the BI-SSb lobe shows silts and sands that have been strongly faulted and folded (Figure 5). Similarly, sediments within one of the moraine ridges in the Otway lobe show faulted sands and gravels (Figure 6). The deformation of moraine sediments in this way is indicative of proglacial glaciotectonism (Rotnicki, 1976; Aber, 1985; Aber et al., 1989; van der Wateren, 1995), and we interpret the deformation to represent thrusting and folding during active re-advances of the ice lobes (Oldale & O'Hara, 1984; Harris et al., 1997; Williams et al., 2001; Evans & Twigg, 2002; Phillips et al., 2002, 2008b, 2008a), at least in these two locations. The BI-SSb moraine contains deformed lacustrine silts, indicating that the timing and extent of retreat and re-advance was sufficient to allow a proglacial lake to accumulate. Our interpretation suggests that some of the moraine ridges may be part of composite thrust complexes, similar to those reported around the Strait of Magellan (Clapperton et al., 1995; Benn & Clapperton, 2000a, 2000b).

4.1.2 Hummocky terrain

Hummocky terrain is abundant within the BI-SSb lobe (Figure 3), but is also found in association with the Magellan lobe (Figure 4). It consists of semi-rounded hills and hollows at both smaller (e.g. ≤ 5 m relief) and larger (> 5 m relief) scales, with the smaller hummocky terrain forming arcuate bands running parallel to moraine ridges. The hummocks are predominantly irregular and chaotic and were classified as ‘irregular hummocky terrain’ (smaller hummocky terrain) and ‘kettle-kame topography’ (larger hummocky terrain) by Darvill et al. (2014).

Hummocky terrain is typically associated with deposition of supraglacial debris (Boulton, 1972; Benn, 1992; Kjaer & Kruger, 2001; Johnson & Clayton, 2003; Schomacker, 2008), although the transport pathway of debris resulting in this terrain is often conjectural (Evans, 2009, and references therein). We infer that the disorganised nature of the landform is indicative of periods of ice stagnation and down-wasting during overall recession of the ice lobes, leaving behind buried ice and resulting in topographic inversion of the terrain (Clayton, 1964; Boulton, 1972; Etzelmüller et al., 1996; Kjaer & Kruger, 2001; Schomacker, 2008). More specifically, the organisation of hummocky terrain in arcuate bands has been interpreted as the product of incremental stagnation (*sensu* Eyles, 1979; Bennett & Evans, 2012) in other lowland settings (e.g. Attig et al., 1989; Ham & Attig, 1996; Clayton et al., 2001; Dyke & Evans, 2003; Evans et al., 2014), a process-form regime that could also apply to the settings described here if the glacier lobes were episodically carrying large englacial and supraglacial debris loads.

Bands of larger hummocky terrain mark the Primera Angostura and Segunda Angostura limits of the Magellan lobe (Meglioli, 1992; Benn & Clapperton, 2000a, 2000b; Rabassa, 2008; Figure 2), but are seen most clearly as a double band on both the north and south sides of the BI-SSb depression (Figures 1, 3, 7). This landform was described as ‘kettle and kame topography’ by (Darvill et al., 2014), but the nomenclature is problematic given that there is no sedimentary evidence for kames and similar features in North America have an ambiguous origin (*sensu* Evans, 2009). Rather, we tentatively group the landform with hummocky terrain and suggest that further sedimentary work is required to establish the full nature of this geomorphology. The topography consists of chaotic hills surrounding rounded hollows, and delimited by broad outwash plains. Darvill et al. (2015a) mapped a series of erratic boulder trains along the southern edge of the BI-SSb lobe, two of which drape over the larger hummocky terrain. A deep section through the inner band of the BI-SSb lobe (the San Sebastián drift) shows two basal diamict units separated by outwash sands and gravels (Figure 7). This implies that the ice lobe advanced to form the outer (Río Cullen) band first before retreating into the BI-SSb depression and subsequently re-advancing.

4.1.3 Geometrical ridges

A large swath of strikingly linear cross-cutting ridges occurs north of Laguna Larga in the central BI-SSb depression. These are regularly-orientated geometrical ridge networks (*sensu* Bennett et al., 1996), described as 'regular hummocky terrain' by Darvill et al. (2014; Figures 3B and 8). They comprise discontinuous, cross-cutting, conjugate paired ridges, generally orientated perpendicular to former ice flow. Although long-regarded as the remnants of crevasse-squeeze ridges, and also diagnostic of glacier surges in a landsystems sense (Raedecke, 1978; Sharp, 1985; Bennett et al., 1996), such landforms have since also been related to: a) active temperate glacier lobes, where they occur in narrow concentric arcs in association with sawtooth style push moraines (Evans & Twigg, 2002; Evans et al., 2015); and b) ice stream shutdown, where they occur in narrow corridors on palaeo-ice stream trunks (Evans et al., 2016). The spatial arrangement of the BI-SSb geometrical ridge networks is identical to the wide arcuate zones of surge-related crevasse-squeeze ridges found on modern glacier forelands, suggesting they may record a phase of glacier surging by the BI-SSb lobe (see discussion).

4.2 Subglacial landforms

4.2.1 Glacial lineations

Lineations occur in association with all five ice lobes, but vary in morphology from low-relief flutings to prominent oval-shaped drumlins. For example, clusters of subdued flutings occur around Bahía Inútil (Raedecke, 1978; Figure 3), whilst large swaths of rounded drumlins are found in the Río Gallegos, Skyring, Otway and Magellan lobes. Of particular note are the fields consisting of hundreds of elongate drumlins that occur in the outermost part of the Río Gallegos lobe (Ercolano et al., 2004; Figure 9), around Laguna Cabeza del Mar in the Otway lobe (Clapperton, 1989; Benn & Clapperton, 2000b; Figure 10C) and on the eastern side of the Magellan Strait (Bentley et al., 2005; Lovell et al., 2012; Figure 4).

The precise genesis of glacial lineations is contentious, but it is generally agreed that they are subglacially streamlined landforms related to the deformation and/or erosion of a soft substrate by fast flowing glacier ice (Stokes et al., 2011). Hence, the lineations in our study area were probably formed by subglacial deformation of glaciofluvial deposits during advances of warm, wet-based ice (Clapperton, 1989; Benn & Clapperton, 2000b). Generally, the lineations are associated with ice marginal features, but a few dense swaths of drumlins occur in isolation from any apparent ice margin and show elements of convergence and divergence, most clearly in the area around Laguna Cabeza del Mar in the Otway lobe (Figure 2). Here, we suggest that the attenuated bedforms, parallel concordance and abrupt lateral margins of the lineation patterns are similar to those in areas of former rapidly flowing ice (Stokes & Clark, 1999, 2001; Evans et al., 2008; Lovell et al., 2012).

4.2.2 Subdued moraine topography

Subdued moraine topography consists of low, arcuate changes in relief (> 1 km wide), often over-printed by other moraine ridges or bands of smaller hummocky terrain. The features are difficult to observe clearly on the ground and are best picked-out as positive relief in SRTM imagery or changes in vegetation in Landsat imagery. Subdued moraine topography is predominantly found in the centre of the BI-SSb lobe and is fragmented in a regular pattern north of Laguna Larga (Raedecke, 1978; Figure 3B).

The regular fracturing of subdued moraine topography north of Laguna Larga could represent linear en echelon deposits linked to crevassing (Raedecke, 1978). However, this is unlikely because the topography is draped by younger features such as moraine ridges, glacial lineations and smaller hummocky terrain. Another possibility is that the subdued moraine topography is similar to the ‘traction ribs’ inferred beneath modern ice masses (Sergienko & Hindmarsh, 2013) and palaeo-ice stream tracks in the southwestern Laurentide Ice Sheet . Given the similarity in orientation to moraine ridges, however, the most likely explanation is that this subdued topography resulted from ice-marginal moraines that were subsequently overridden and moulded subglacially, similar to landforms (overridden moraines) observed in Iceland (Krüger, 1994; Evans & Twigg, 2002; Evans & Orton, 2015; Evans et al., 1999; Evans, 2009; Evans et al., 2015).

4.2.3 Irregular dissected ridges

A series of disorganised ridges, in places intersected by meltwater channels, are found in association with the Skyring and Río Gallegos lobes, most prominently to the southeast of the large swath of drumlins oriented southeastward in the Río Gallegos lobe (Flow-set 1: FS 1; Figure 9). The origin of the features is unclear, although the largest group appears to be situated at the intersection between the former Río Gallegos and Skyring ice lobes.

We suggest that the Río Gallegos lobe advanced first into the area, creating a drumlin field and moraine ridges. Subsequently, the Río Gallegos lobe retreated and the Skyring lobe advanced over the drumlins and moraines, causing subglacial deformation that resulted in an irregular pattern of hills and meltwater channels. The stratigraphic order is indicated by meltwater from the Skyring lobe draining into the Río Gallegos depression.

4.3 Glaciofluvial landforms

4.3.1 Meltwater channels

The study area is dominated by meltwater features, including hundreds of sinuous channels. In places, such as the outer moraines of the Skyring, Otway and Magellan lobes, the channels flow between moraine ridges (Figure 2), but elsewhere, such as the BI-SSb depression and inner parts of the Río Gallegos, Skyring, Otway and Magellan lobes, meltwater channels are clearer than the associated moraines (Bentley et al., 2005). The channels vary in size, from less than 50 m wide to more than 150 m wide, and are sometimes associated with channels of outwash where ice overtopped topographic constraints (e.g. northeast of the Skyring and Otway lobes or north of the BI-SSb lobe).

4.3.2 Outwash plains

Outwash plains were identified based on their relatively smooth, featureless appearance, whose surfaces gently grade downslope from former ice margins. The plains are associated with moraines and hummocky terrain in all of the ice lobes, and (where they are unconstrained by topography) wide, open sandur plains grade eastward. A prominent exception is the outwash plain originating from Laguna Blanca in the Skyring lobe (Figures 2 and 10), which trends south-eastward into the Strait of Magellan and surrounds a former moraine belt associated with the Otway lobe (Lovell et al., 2012).

The extensive nature of the glaciofluvial features implies that all of the ice lobes produced large quantities of meltwater during stillstands and retreat. Whilst meltwater channels and outwash plains are abundant within the study area, features such as ice contact fans, pitted outwash plains and eskers are not. Indeed, there is a notable absence of eskers associated with the ice lobes, which might imply that meltwater was rarely routed into conduits at the bed (perhaps draining into the substrate or maybe as a result of cold-based ice) or that there was insufficient time for conduits to form (Storrar et al., 2014a, 2014b). Alternatively, ice-walled deposition may have been restricted to englacial settings, in a similar fashion to the receding lowland lobes of Iceland, where drainage bypasses overdeepenings and hence eskers emerge on the surface of downwasting snouts (Spedding & Evans, 2002; Bennett et al., 2010; Bennett & Evans, 2012). Such a scenario would result in tunnel fills being significantly reworked during deglaciation and consequently difficult to identify in the landform record.

4.4 Proglacial lake landforms

4.4.1 Former shorelines

Numerous fragmentary shorelines are found within *ca*. 10 m elevation of contemporary coastal areas. In addition, continuous shorelines are found above 10 m and, further inland, around Lago Balmaceda in the Río Gallegos lobe (Figure 1); Seno Skyring; Seno Otway (Figure 2); Laguna Blanca in the Skyring lobe (Figure 10A); south of Primera Angostura in the Strait of Magellan (Figure 4); and Bahía Inútil (Figure 3A). Whilst the Skyring, Otway, Magellan and Bahía Inútil shorelines are generally within 30 m of present-day sea-level, those around Lago Balmaceda and Laguna Blanca are substantially higher.

Our glacial reconstruction, combined with DEM modelling, and the occurrence of localised palaeolacustrine sedimentary evidence, leads us to infer that these shorelines relate to a total of six large proglacial lakes that existed at various times in the overdeepenings in front of the former ice lobes. This reconstruction supports previous work on proglacial lake reconstruction in the area (Porter et al., 1992; Clapperton et al., 1995; McCulloch et al., 2005a; Sagredo et al., 2011; Stern et al., 2011; Lovell et al., 2012; Kilian et al., 2007, 2013). The ice-marginal truncation of these shorelines suggests that they formed in front of the ice lobes, likely during recession into their respective topographic basins/overdeepenings.

5 Style and dynamics of Quaternary glaciation

5.1 Active temperate glacial landsystem

The majority of the glacial geomorphology in the study area can broadly be divided into three landform assemblages: morainic, subglacial and glaciofluvial (Figure 11). The components of each assemblage as well as their inter-relationships are consistent with an active temperate glacial landsystem developed during the advance and retreat of the ice lobes (Evans & Twigg, 2002). The warm-based active recession of this landsystem produces three characteristic landform-sediment associations. Firstly, dump, push and squeeze moraines composed of proglacial sediments mark the ice limit, sometimes displaying annual signatures or evidence for stillstands that create stacked features (Price, 1970; Evans et al., 1999; Evans & Twigg, 2002; Evans et al., 2015). Low amplitude ridges formed from overridden push moraines may also be found, draped by glacial lineations and moraines. Secondly, subglacially streamlined flutings and drumlins occur between these moraines. Thirdly, extensive glaciofluvial landforms occur where meltwater flows away from the warm-based ice front. These features include ice-contact and spillway-fed outwash fans; ice marginal outwash tracts; kame terraces; pitted outwash and eskers (Evans & Twigg, 2002; Evans, 2003b). Active temperate glaciers are also capable of constructing arcuate bands of hummocky moraine during recession as a result of incremental stagnation, driven by pulses of supraglacial debris (Eyles, 1979; Bennett & Evans, 2012). The geomorphology in the central part of the BI-SSb lobe (Figure 11) displays many of the landforms associated with an active temperate landsystem: moraines containing proglacially-thrusted and folded sediments; possible recessional push moraines; overridden moraines; flutings and drumlins; and glaciofluvial meltwater channels and outwash plains.

The similarity between the landform assemblages in our study area and those associated with active temperate glaciers supports the assertion that the ice lobes dominantly operated under an active temperate glacial landsystem. This is especially clear in the geomorphology of the central BI-SSb lobe. The other ice lobes show the characteristics associated with active temperate glaciers, but the geomorphology is either not as well preserved (as in the Río Gallegos and Magellan lobes) or the moraines are more tightly nested (as in the Skyring and Otway lobes) so that the assemblages are not as clear. Tightly nested moraine sequences may indicate that the Skyring and Otway lobes retreated more slowly than the other ice lobes, although there are no chronological constraints on the rate of this recession (see Section 6.2). Similar patterns of tightly nested features have been observed in Iceland (Bradwell et al., 2013), but, in our study, the cause may be related to topographic constraints, rather than annual cycles in retreat (Kaplan et al., 2009; Anderson et al., 2012; Barr & Lovell, 2014). Hence, the landform assemblages of the Skyring and Otway lobes may be indicative of an active temperate landsystem, but they are not as clear as the BI-SSb lobe due to slower glacier recession.

5.2 External forcing of glacier behaviour

There are a number of implications associated with our interpretation of an active temperate glacial landsystem. Principally, Benn & Clapperton (2000a, 2000b) suggested that the Magellan lobe operated under subpolar conditions, with a cold-based margin, during the gLGM. By contrast, Bentley et al. (2005) advocated warm-based conditions extending to the ice margin based on different glacier limits that implied steeper ice surface gradients. The presence of proglacially thrust moraines and arcuate bands of hummocky terrain, if they originated as controlled ridges (*sensu* Evans, 2009), are consistent with cold-based ice or at least a polythermal basal regime (Benn & Clapperton, 2000b; Evans, 2009). Evidence for glacial lineations extending to individual moraine ridges is a landform association indicative of warm-based ice throughout the snout (Evans & Twigg, 2002; Evans, 2003b), and arcuate hummocky terrain bands set within recessional push moraines are consistent with phases of incremental stagnation by temperate glaciers. However, glacial thermal regimes form a continuum upon which the landsystem signatures of polythermal glaciers, with frozen snouts (e.g. Svalbard valley glaciers and Icelandic upland icefields), and active temperate glaciers, with winter frozen toe zones and pulsed supraglacial debris transfer, would be difficult to differentiate (Evans, 2009). Particularly significant for southernmost Patagonia is the independent evidence for permafrost conditions at the gLGM (Benn & Clapperton, 2000a, 2000b; Bockheim et al., 2009). Therefore, we suggest that the former ice lobes were predominantly active temperate in nature, but were subject to periods of polythermal conditions, thereby giving rise to phases of controlled moraine construction. A similar scenario has been proposed for the southern limits of the Laurentide Ice Sheet in the interior plains of North America (Clayton et al., 2001; Colgan et al., 2003; Bauder et al., 2005; Evans et al., 2006, 2014). This further illustrates the importance of recognising what Evans (2013) identifies as landsystem superimposition and spatio-temporal change, whereby changes in the climatic environment occupied by a glacier will inevitably be reflected in its geomorphic signature. The incremental stagnation versus controlled origin of the hummocky terrain arcs is important to the palaeoglaciological reconstruction and its palaeoclimatic inferences made above, and therefore needs to be vigorously tested by future sedimentological investigations.

The complex landform-sediment signatures of the southernmost Patagonian outlet lobes are indicative of active temperate glaciers. Such glaciers are characterised by active advance during periods of overall recession, primarily controlled by regional climatic variability (Colgan et al., 2003; Evans, 2003b, 2011; Evans & Orton, 2015; Evans et al., 2015). Modern examples include Breiðamerkurjökull, Fjallsjökull, Heinabergsjökull, Skalafellsjökull and Fláajökull in Iceland (Evans & Twigg, 2002; Evans et al., 2015; Evans & Orton, 2015; Evans, 2003b). Both topographic control (Kaplan et al., 2009; Anderson et al., 2012; Barr & Lovell, 2014) and internal ice dynamics (Benn & Clapperton, 2000a, 2000b; Lovell et al., 2012) have also been proposed as factors controlling glacial activity within this region. Our geomorphological evidence implies that, for the majority of ice fluctuations, these internal forcing factors may have been of secondary importance to climatic variability.

5.3 Internal forcing of glacier behaviour

Whilst the landform evidence suggests that the ice lobes predominantly advanced and retreated according to an externally-forced active temperate landsystem, there is also evidence for periods of rapid ice flow and proglacial lake development. Both of these situations may have temporarily interrupted the primary climatic driver of glacial activity.

5.3.1 Transient rapid ice flow

A large swath of elongated, closely-spaced drumlins in the inner part of the Otway lobe around Laguna Cabeza del Mar (FS 8 in Figure 12) has previously been hypothesised to represent rapid ice flow (Benn & Clapperton, 2000b; Lovell et al., 2012). Unlike other glacial lineations in the study area, this drumlin field resembles a terrestrial palaeo-ice stream, with convergent flowlines, attenuated bedforms and abrupt lateral margins (Stokes & Clark, 1999; Clark & Stokes, 2003; Lovell et al., 2012). Additionally, Lovell et al. (2012) raised the possibility for surge-like behaviour of the Otway lobe based partly on this landform evidence. Our study confirms that many of the landforms associated with surging activity are exhibited in the study area, including thrust moraines, highly elongate flutings, hummocky terrain and crevasse-squeeze ridges, which are often viewed as diagnostic of surge activity (Evans & Rea, 1999, 2003; Schomacker et al., 2014; Lovell et al., 2015). As such, we suggest the ice lobes may have periodically displayed rapid ice-flow and possible surge-like behaviour.

Our reconstruction of fast-flowing ice would have affected ice dynamics in parts of the ice lobes. Similar fast-flowing systems in northern Patagonia during the gLGM are hypothesised to have resulted in greater ice discharge rates (Glasser & Jansson, 2005), and rapid ice flow across much of the eastern portion of the Patagonian Ice Sheet may help to explain mismatches between model outputs and landform reconstructions (Hulton et al., 2002; Glasser & Jansson, 2005). The presence of landforms linked to possible surge-like advances further implies that, at times, the ice lobes may have briefly advanced in response to non-climatic forcing. The possible evidence for palaeo-surges warrants further research, particularly given the paucity of examples of surging systems in the palaeo-record and the fact that some contemporary active temperate glaciers, such as Breiðamerkurjökull, have also displayed surging activity and this is recorded in landsystem overprinting (Evans & Twigg, 2002).

5.3.2 Proglacial lake development

The clearest proglacial lake landforms are within the Skyring lobe, where meltwater accumulated above the present day Laguna Blanca. Shorelines and DEM modelling indicate a maximum lake surface elevation of *ca*. 190 m.a.s.l., which drained northward into the basin previously occupied by the Río Gallegos lobe (Lovell et al., 2012; Figure 10A and B). This reconstruction is supported by sedimentological evidence northeast of Laguna Blanca consisting of rhythmically laminated silt and clay sediments, containing dropstones (Figure 10E). Our ice limit for the Otway lobe differs from Lovell et al. (2012), such that a similar proglacial lake did not form in front of the Otway lobe because meltwater could drain southeastward in front of the Magellan lobe. Once the Skyring lobe retreated beyond the topographic bluff separating it from the Otway lobe, drainage of the palaeo-Laguna Blanca proglacial lake switched from a northward to a south-eastward direction, in front of the Otway and Magellan lobes and into the Strait of Magellan (Figure 10C and F). The drainage resulted in the formation of large meltwater channels and an associated outwash plain that surrounded a moraine belt associated with the Otway lobe.

Proglacial lakes are also reconstructed in front of the BI-SSb and Magellan lobes (Figure 13), consistent with the presence of lacustrine sediments (McCulloch et al., 2005a). The BI-SSb lake reached approximately 20 m.a.s.l. before draining at Onaisín, eastward toward the Atlantic through a channel now marked by Laguna Larga (Figure 3A and B). Likewise the Magellan lake drained eastward toward the Atlantic, but the height of the lake is less clear as the drainage channel is below present day sea-level (Porter et al., 1992; Clapperton et al., 1995; McCulloch et al., 2005a). Our reconstruction suggests that at its peak the lake extended onto the low plain in front of the Otway lobe. Small lakes also formed at 10-20 m.a.s.l. on the eastern flank of the Magellan lobe, north of Porvenir (Figure 4B). One of these lakes deposited a large section of rhythmically laminated silt and clay sediments at Laguna Verde (Figures 10G, H, I and 4B).

A proglacial lake formed in front of the Otway lobe once ice had retreated into the present-day Seno Otway, and there is evidence for a channel initially draining north-eastward into the Strait of Magellan (Mercer, 1976; McCulloch et al., 2005a). However, once the lake level dropped to around 20 m.a.s.l., drainage would have switched to the northwest through Canal Fitzroy into a similar lake at 10-20 m.a.s.l. within present-day Seno Skyring (Figure 2). The Skyring proglacial lake drained northward through Estero Obstrucción (Figure 1) into a large lake in front of the Río Gallegos lobe, the extent of which is unclear (Sagredo et al., 2011; Stern et al., 2011), although final drainage of the Otway, Skyring and Río Gallegos lakes would have been westward through Golfo Almirante Montt (Figure 1) once ice had receded into the mountains (McCulloch et al., 2005a; Stern et al., 2011).

Former proglacial lakes would also have affected glacial dynamics by promoting increased rates of ice retreat (Porter et al., 1992; Teller, 2003; Lovell et al., 2012; Carrivick & Tweed, 2013). The presence of a proglacial lake at the margin of a glacier can trigger positive feedbacks such as increased englacial water pressure and temperature; increased subglacial pressure; and increased ice surface gradients, which can result in calving, ice-margin flotation and the flushing of sediment from beneath the ice (Carrivick & Tweed, 2013). This results in greater ice mass loss and glacial draw-down (Lovell et al., 2012). Porter et al. (1992) also suggested that calving of the Magellan and BI-SSb lobes could have resulted in a rapid loss of ice. Given the potential importance of proglacial lakes in controlling ice dynamics within this region, future work should aim to better constrain their evolution over time.

6 Glacial reconstruction and timing

6.1 Glacial limits and flow-sets

Three sets of ice-marginal landforms were used to demarcate former glacial limits: morainic landforms (including hummocky terrain), glacial lineation flow-sets (see below), and meltwater channels. The different lines of evidence yielded a consistent pattern and the data were synthesised to create a map of prominent limits for each ice lobe (Figure 12). Many of these limits corroborate previous work defining glacial limits in the region (Meglioli, 1992; Clapperton et al., 1995; Coronato et al., 2004; Bentley et al., 2005; Lovell et al., 2012), but the wider scope of our mapping reveals a more detailed pattern than has been previously reported. For comparison, we also included less extensive limits from Kilian et al. (2007) for the Skyring lobe (Figure 12D).

A total of 20 flow-sets (FS) were identified within the study area (Figure 12B), with those of the Skyring and Otway lobes similar to Lovell et al. (2012). An exception is the separation of FS 7 and 8 based on differing morphology: the drumlins around Laguna Cabeza del Mar are noticeably longer, wider, and higher than the long flutings further to the northeast. This division is important because FS 8 corresponds with moraines dissecting the Otway depression. Some flow-sets within the inner parts of the Río Gallegos, Skyring, Magellan and BI-SSb lobes have been discussed in previous studies (Benn & Clapperton, 2000b; Ercolano et al., 2004; Bentley et al., 2005; Lovell et al., 2012), but the outer flow-sets of the Río Gallegos and BI-SSb lobes have not been reported previously.

The glacial limits that we have defined can be used to reconstruct a relative sequence of events in the glacial history, enhanced by information about ice dynamics from our landsystems approach. Correlating between the limits of adjacent ice lobes can be problematic because they are generally reconstructed from fragmentary records, and joining-up limits can over-emphasise correlation without robust chronological controls. However, in places, our approach informs the relative timing of advance and retreat between lobes based on cross-cutting landform assemblages. Using cross-cutting relationships between flow-sets and ice marginal landform assemblages, we identify eight separate relative time steps in our reconstruction (Figure 13). These time steps are shown in relation to present-day basal topography and the height of former proglacial lakes in Figure 14. We now briefly discuss key aspects of the nature and timing of this glacial history in relation to the eight time steps and a compilation of recalibrated chronological information (Figure 15).

6.2 Chronological framework

This study is principally engaged with reconstructing the dynamics of former ice lobes without considering time-dependent variation. However, it is possible and informative to place our time steps within a framework of previously published chronological data (Figures 13 and 15). Full details of this chronological compilation, including calibration and recalculation methods, are given in the Supplementary Material and Tables S1, S2, S3 and S4.

6.2.1 Time steps 1-4: Pre-gLGM advances

There is uncertainty regarding the ages of pre-gLGM glacial limits within the study area (time steps 1-4 in our reconstruction). Cosmogenic nuclide exposure dating of boulders from moraines of the BI-SSb, Magellan and Río Gallegos lobes (Kaplan et al., 2007; Evenson et al., 2009) has yielded ages that are substantially younger than associated $^{40}Ar/^{39}Ar$ dates from nearby volcanic flows (Figure 13A, B and C; (Meglioli, 1992; Singer et al., 2004), the cause of which is contentious (Kaplan et al., 2007; Darvill et al., 2015a). Darvill et al. (2015b) used $^{10}Be/^{26}Al$ depth profiles through outwash sediments to show that two limits previously assigned to older glacial stages were deposited during the last glacial cycle. Overall, the large spread of boulder ages associated with time steps 1-4 may result from post-depositional processes such as boulder erosion (Kaplan et al., 2007) and the gradual melt-out of dead ice in hummocky terrain (Schomacker, 2008; Darvill et al., 2015a).

In time step 4, the BI-SSb lobe re-advanced to close to the limit of time step 3 (Figure 14), with ^{10}Be dates from boulders of 24.3 ka and 224.1 ka (Figures 13D; Kaplan et al., 2007). A depth-profile through associated outwash yielded a more robust age of 30.1 ka (Darvill et al., 2015b). For the Magellan lobe, eight ^{10}Be ages between 24.8 ka and 36.9 ka and two ^{26}Al ages of 31.0 ka and 32.6 ka (Kaplan et al., 2007) imply that the limit may have been deposited at a similar time to that of the BI-SSb lobe (Figure 15).

6.2.2 Time steps 5-6: Re-advances, rapid flow and lake drainage

The Otway lobe re-advanced significantly during time step 5 (Figure 13E), forming FS 8 around Laguna Cabeza del Mar and shifting the ice divide between the Otway and Magellan lobes south-eastward into the present-day Strait of Magellan. The BI-SSb lobe also re-advanced to a limit close to Bahía San Sebastián, depositing a large terminal moraine that is still preserved east of Laguna Larga (Figure 3) and forming FS 17 (Figure 13E). The re-advances of these two ice lobes may have been in response to rapid ice flow (and possible surge-like activity based on the presence of thrust moraines, highly elongate flutings, hummocky terrain and crevasse-squeeze ridges). The Río Gallegos, Magellan and Skyring lobes retreated during time step 5, with the latter developing a proglacial lake – palaeo-Laguna Blanca – which may have further facilitated ice loss through calving (Figures 13E and 14). However, there are no direct age constraints for this time step. Recession continued during time step 6, allowing the potentially catastrophic drainage of palaeo-Laguna Blanca from in front of the Skyring lobe east to south-easterly in front of the Otway and Magellan lobes (Figure 13F). The drainage event is important because it acts as a stratigraphic tie-point for all three ice lobes (Figure 15). As mentioned in Section 6.2.1, ages of 24.8 ka and 36.9 ka for the Magellan lobe at Primera Angostura (Figure 2) suggest that it advanced prior to the gLGM during the last glacial cycle. The lake drainage is constrained by these ages and four more ^{10}Be ages of 27.4 ka to 29.9 ka on Península Juan Mazía (McCulloch et al., 2005b; Kaplan et al., 2008a). The implication is that the Skyring, Otway and Magellan lobes were all retreating from more extensive positions prior to the gLGM (Figure 15).

6.2.3 Time step 7: The gLGM

During time step 7, the ice lobes reached positions that have been broadly correlated with the gLGM (Figures 13G and 15). Based upon our landform evidence (e.g. highly elongate flutings and hummocky terrain), the Magellan lobe readvance may have been surge-like, and has been ^{10}Be dated to between 18.3 ka and 23.2 ka. The BI-SSb lobe readvance has also been ^{10}Be, ^{26}Al and ^{36}Cl dated to between 15.6 ka and 55.8 ka (though sixteen ^{10}Be dates were between 17.6 ka and 24.9 ka; McCulloch et al., 2005b; Kaplan et al., 2007, 2008a; Evenson et al., 2009). The reason for the scatter in ages is unclear, although the ^{10}Be date of 55.8 ka may be due to inheritance, given that most of the dates are from a large erratic boulder train on the south-eastern side of Bahía Inútil (Darvill et al., 2015a). There are no supporting ages for the Río Gallegos, Skyring and Otway lobes but they were likely situated within the present-day fjords.

6.2.4 Time step 8: Rapid retreat

All of the ice lobes were in post-gLGM retreat during time step 8 (Figure 13H), developing proglacial lakes in front of their receding margins that likely increased the rate of ice loss through calving (Figure 14; Porter et al., 1992; Kilian et al., 2007; Carrivick & Tweed, 2013). The Magellan and BI-SSb proglacial lakes drained eastward toward the Atlantic, although their extent is uncertain. Drainage of the Otway proglacial lake initially occurred east to north-eastward into the Magellan lake, but as lake levels dropped during ice retreat, drainage switched to north-westward into the Skyring proglacial lake, cutting the Fitzroy channel (McCulloch et al., 2005a; Kilian et al., 2013). In turn, the Skyring proglacial lake drained into the Río Gallegos proglacial lake that, by this time, may have drained westward into the Pacific Ocean through ice-free fjords dissecting the Andes (McCulloch et al., 2005a; Kilian et al., 2013). It is possible that Río Gallegos ice was still extensive, such that drainage occurred in a southwards direction, reaching the Pacific through Seno Otway (Stern et al., 2011). Ultimately, uncertainty in the configuration of the Río Gallegos lobe makes it difficult to assess drainage routes.

Ice-free conditions in Seno Skyring and Seno Otway have been dated to at least 14.8 ka and 14.7 ka, respectively, based on radiocarbon dating and tephrostratigraphy of sediment cores (Kilian et al., 2013). The Skyring lobe may have been undergoing rapid retreat linked in part to calving (Kilian et al., 2007). Numerous radiocarbon dates suggest that retreat of the Magellan and BI-SSb ice lobes was also under way by at least 14-15 ka (Porter et al., 1992; Anderson & Archer, 1999; Clapperton et al., 1995; McCulloch & Bentley, 1998; McCulloch et al., 2005b), although the presence of the Reclús tephra within lake sediments implies that full retreat and final proglacial lake drainage cannot have been before *ca*. 14.3 ka (McCulloch et al., 2005a). The rapid retreat, and possible collapse, of the BI-SSb lobe is supported by radiocarbon dates as early as 16.8 ka in central Cordillera Darwin (Hall et al., 2013; Figure 15). A similarly rapid retreat is reconstructed for the Magellan lobe (Figure 15), likely linked to the broad calving termini of these ice lobes (Porter et al., 1992).

7 Conclusions

This study presents a reconstruction of the relative history of five former ice lobes in southernmost South America. We reconstruct eight time steps, which highlight the dynamic nature of this part of the ice sheet margin, and use a landsystem approach to show that the ice lobes dominantly displayed behaviour similar to active temperate glaciers. This involved warm-based ice actively re-advancing during overall retreat of the ice margin and questions previous hypotheses that the ice lobes displayed sub-polar characteristics with cold-based margins. The implication is that active temperate ice lobes would have been primarily controlled by regional climate variability. Superimposed on these active temperate landsystems are areas where swaths of elongated, closely-spaced drumlins and suites of landforms including possible crevasse-squeeze ridges suggest periodically rapid ice flow, perhaps indicative of some readvances linked to surge-like activity. Additionally, our reconstruction highlights the importance of the palaeo-Laguna Blanca proglacial lake, which developed in front of the Skyring lobe, and drained, potentially catastrophically, prior to the gLGM. The development of other proglacial lakes in front of all of the ice lobes following the gLGM would have promoted calving and rapid retreat, or collapse, of the ice margins.

For the Río Gallegos, Skyring and Otway lobes, existing age constraints are scarce and contradictory, but our recalculation of dates for older positions of the Magellan lobe suggests that at least one limit of greater extent than the gLGM limit was deposited around 30 ka. This suggests that the BI-SSb and Magellan lobes advanced in a similar manner and at similar times. Similarity in the timing of ice advances from the available chronological information implies that, broadly speaking, ice lobe response was primarily controlled by climate variability, supporting a model of active temperate glaciation. However, additional chronological controls are needed to test this model further, particularly for the Río Gallegos, Skyring and Otway lobes.

8 Acknowledgments

CMD would like to thank Will Christiansen, Mark Hulbert and Paul Lincoln for their assistance and companionship in the field, as well as Jorge Rabassa, Andrea Coronato and Juan Carlos Aravena for fieldwork support and guidance. This research was funded by a UK NERC Ph.D. studentship (NE/j500215/1) awarded to CMD at Durham University. Fieldwork was also supported by an Explorers Club Exploration Grant, Quaternary Research Association NRW Award, Santander Mobility Grant, the Durham University Faculty of Social Sciences and Health, Durham University Geography Department, and a UK NERC Ph.D. studentship (NE/I528050/1) awarded to HL at Queen Mary University of London. Additionally, the Ph.D. research of CMD was assisted by a Royal Geographical Society

Dudley Stamp Memorial Award and British Society for Geomorphology Postgraduate Research Grant, as well as funding from the Norman Richardson Postgraduate Research Fund and an Ustinov College Travel Grant at Durham University. We are grateful to Neil Glasser for comments on an early version of this manuscript and to Andrew Lorrey for his editorial work on the published version. This paper benefitted greatly from the detailed and considered comments of three anonymous reviewers.

9 References

Aber, J. (1985). The character of glaciotectonism. *Geologie en Mijnbouw* **64**, 389–395.

Aber, J., Croot, D. & Fenton, M. (1989). *Glaciotectonic Landforms and Structures*. Dordrecht: Kluwer Academic Publishers.

Anderson, D.M. & Archer, R.B. (1999). Preliminary evidence of early deglaciation in southern Chile. *Palaeogeography Palaeoclimatology Palaeoecology* **146** (1-4), 295–301.

Anderson, R.S., Dühnforth, M., Colgan, W. & Anderson, L. (2012). Far-flung moraines: Exploring the feedback of glacial erosion on the evolution of glacier length. *Geomorphology* **179**, 269–285.

Attig, J.W., Mickelson, D.M. & Clayton, L. (1989). Late Wisconsin landform distribution and glacier-bed conditions in Wisconsin. *Sedimentary Geology* **62** (2-4), 399–405.

Barr, I.D. & Lovell, H. (2014). A review of topographic controls on moraine distribution. *Geomorphology* **226**, 44–64.

Bauder, A., Mickelson, D.M. & Marshall, S.J. (2005). Numerical modeling investigatonsof the subglacial conditions of the southern Laurentide ice sheet. *Annals of Glaciology* **40** (1987), 219–224.

Benn, D.I. (1992). The genesis and significance of ‘hummocky moraine’: Evidence from the Isle of Skye, Scotland. *Quaternary Science Reviews* **11** (7-8), 781–799.

Benn, D.I. & Clapperton, C.M. (2000a). Glacial sediment-landform associations and paleoclimate during the last glaciation, Strait of Magellan, Chile. *Quaternary Research* **54** (1), 13–23.

Benn, D.I. & Clapperton, C.M. (2000b). Pleistocene glacitectonic landforms and sediments around central Magellan Strait, southernmost Chile: evidence for fast outlet glaciers with cold-based margins. *Quaternary Science Reviews* **19** (6), 591–612.

Bennett, G.L. & Evans, D.J.A. (2012). Glacier retreat and landform production on an overdeepened glacier foreland: the debris-charged glacial landsystem at Kvíárjökull, Iceland. *Earth Surface Processes and Landforms* **37** (15), 1584–1602.

Bennett, G.L., Evans, D.J.A., Carbonneau, P. & Twigg, D.R. (2010). Evolution of a debris-charged glacier landsystem, Kvíárjökull, Iceland. *Journal of Maps* **6** (1), 40–67.

Bennett, M.R., Hambrey, M.J., Huddart, D. & Ghienne, J.F. (1996). The formation of a geometrical ridge network by the surge-type glacier Kongsvegen, Svalbard. *Journal of Quaternary Science* **11** (6), 437–449.

Bentley, M.J., Sugden, D.E., Hulton, N.R.J. & McCulloch, R.D. (2005). The landforms and pattern of deglaciation in the Strait of Magellan and Bahia Inútil, southernmost South America. *Geografiska Annaler Series a-Physical Geography* **87A** (2), 313–333.

Blomdin, R., Murray, A., Thomsen, K.J., Buylaert, J.-P., Sohbati, R., Jansson, K.N. & Alexanderson, H. (2012). Timing of the deglaciation in southern Patagonia: Testing the applicability of K-Feldspar IRSL. *Quaternary Geochronology* **10** (0), 264–272.

Bockheim, J., Coronato, A., Rabassa, J., Ercolano, B. & Ponce, J. (2009). Relict sand wedges in southern Patagonia and their stratigraphic and paleo-environmental significance. *Quaternary Science Reviews* **28** (13-14), 1188–1199.

Boulton, G.S. (1972). Modern Arctic glaciers as depositional models for former ice sheets. *Journal of the Geological Society* **128** (4), 361–393.

Bradwell, T., Sigurdsson, O. & Everest, J. (2013). Recent, very rapid retreat of a temperate glacier in SE Iceland. *Boreas* **42** (4), 959–973.

Caldenius, C.C. zo. (1932). Las Glaciaciones Cuaternarias en la Patagonia y Tierra del Fuego. *Geografiska Annaler* **14**, 1–164.

Caniupán, M., Lamy, F., Lange, C.B., Kaiser, J., Arz, H., Kilian, R., Baeza Urrea, O., Aracena, C., Hebbeln, D., Kissel, C., Laj, C., Mollenhauer, G. & Tiedemann, R. (2011). Millennial-scale sea surface temperature and Patagonian Ice Sheet changes off southernmost Chile (53°S) over the past 60 kyr. *Paleoceanography* **26** (3), n/a–n/a.

Carrivick, J.L. & Tweed, F.S. (2013). Proglacial lakes: character, behaviour and geological importance. *Quaternary Science Reviews* **78**, 34–52.

Clapperton, C.M. (1989). Asymmetrical drumlins in Patagonia, Chile. *Sedimentary Geology* **62** (2–4), 387–398.

Clapperton, C.M. (1993). *Quaternary geology and geomorphology of South America*. B.V., Amsterdam: Elsevier Science Publishers.

Clapperton, C.M., Sugden, D.E., Kaufman, D.S. & McCulloch, R.D. (1995). The Last Glaciation in Central Magellan Strait, southernmost Chile. *Quaternary Research* **44** (2), 133–148.

Clark, C.D. (1999). Glaciodynamic context of subglacial bedform generation and preservation. *Annals of Glaciology* **28** (1), 23–32.

Clark, C.D. & Stokes, C.R. (2003). Palaeo-ice stream landsystem. In: D. J. A. Evans (ed.). *Glacial Landsystems*. 204–227, London: Hodder Arnold.

Clark, P.U., Dyke, A.S., Shakun, J.D., Carlson, A.E., Clark, J., Wohlfarth, B., Mitrovica, J.X., Hostetler, S.W. & McCabe, A.M. (2009). The Last Glacial Maximum. *Science* **325** (5941), 710–714.

Clayton, L. (1964). Karst topography on stagnant glaciers. *Journal of Glaciology* **5**, 107–112.

Clayton, L., Attig, J.W. & Mickelson, D.M. (2001). Effects of late Pleistocene permafrost on the landscape of Wisconsin, USA. *Boreas* **30** (3), 173–188.

Colgan, P.M., Mickelson, D.M. & Cutler, P.M. (2003). Ice-marginal terrestrial landsystems: southern Laurentide Ice Sheet margin. In: D. J. A. Evans (ed.). *Glacial Landsystems*. 111–142, London: Hodder Arnold.

Coronato, A., Martínez, O. & Rabassa, J. (2004). Glaciations in Argentine Patagonia, southern South America. In: J. Ehlers & P. L. Gibbard (eds.). *Developments in*

Quaternary Sciences. **2**, 49–67, Elsevier.

Coronato, A.M.J., Coronato, F., Mazzoni, E. & Vázquez, M. (2008). The Physical Geography of Patagonia and Tierra del Fuego. In: J. Rabassa (ed.). *Developments in Quaternary Sciences*. **11**, 13–55, Elsevier.

Darvill, C.M., Bentley, M.J. & Stokes, C.R. (2015a). Geomorphology and weathering characteristics of erratic boulder trains on Tierra del Fuego, southernmost South America: Implications for dating of glacial deposits. *Geomorphology* **228**, 382–397.

Darvill, C.M., Bentley, M.J., Stokes, C.R., Hein, A.S. & Rodés, Á. (2015b). Extensive MIS 3 glaciation in southernmost Patagonia revealed by cosmogenic nuclide dating of outwash sediments. *Earth and Planetary Science Letters* **429**, 157–169.

Darvill, C.M., Stokes, C.R., Bentley, M.J. & Lovell, H. (2014). A glacial geomorphological map of the southernmost ice lobes of Patagonia: the Bahía Inútil – San Sebastián, Magellan, Otway, Skyring and Río Gallegos lobes. *Journal of Maps* **10** (3), 500–520.

Doughty, A.M., Schaefer, J.M., Putnam, A.E., Denton, G.H., Kaplan, M.R., Barrell, D.J.A., Andersen, B.G., Kelley, S.E., Finkel, R.C. & Schwartz, R. (2015). Mismatch of glacier extent and summer insolation in Southern Hemisphere mid-latitudes. *Geology* **43** (5), 407–410.

Douglass, D.C., Singer, B.S., Kaplan, M.R., Mickelson, D.M. & Caffee, M.W. (2006). Cosmogenic nuclide surface exposure dating of boulders on last-glacial and late-glacial moraines, Lago Buenos Aires, Argentina: Interpretive strategies and paleoclimate implications. *Quaternary Geochronology* **1** (1), 43–58.

Dyke, A.S. & Evans, D.J.A. (2003). Ice-marginal terrestrial landsystems: Northern Laurentide and Innuitian ice sheet margins. In: D. J. A. Evans (ed.). *Glacial Landsystems*. 143–165, London: Hodder Arnold.

Eaves, S.R., N. Mackintosh, A., Winckler, G., Schaefer, J.M., Alloway, B. V. & Townsend, D.B. (2016). A cosmogenic 3He chronology of late Quaternary glacier fluctuations in North Island, New Zealand (39°S). *Quaternary Science Reviews* **132**, 40–56.

Ercolano, B., Mazzoni, E., Vazquez, M. & Rabassa, J. (2004). Drumlins and drumlinoid forms of the Lower Pleistocene in southern Patagonia, Province of Santa Cruz. *Rev. Asoc. Geol. Argent.* **59** (4), 771–777.

Etzelmüller, B., Hagen, J., Vatne, G., Ødegård, R. & Sollid, J. (1996). Glacial debris accumulation and sediment deformation influenced by permafrost: examples from Svalbard. *Annals of Glaciology* **22**, 53–62.

Evans, D.J.A. (2009). Controlled moraines: origins, characteristics and palaeoglaciological implications. *Quaternary Science Reviews* **28** (3–4), 183–208.

Evans, D.J.A. (2013). Geomorphology and Retreating Glaciers. In: R. Giardino & J. Harbor (eds.). *Treatise on Geomorphology*. 460–478, Elsevier.

Evans, D.J.A. (2003a). *Glacial Landsystems*. Hodder Arnold, London.

Evans, D.J.A. (2011). Glacial landsystems of Satujökull, Iceland: A modern analogue for glacial landsystem overprinting by mountain icecaps. *Geomorphology* **129** (3-4), 225–237.

Evans, D.J.A. (2003b). Ice marginal terrestrial landsystems: Active temperate glacier margins. In: D. J. A. Evans (ed.). *Glacial Landsystems*. 12–43, London: Hodder Arnold.

Evans, D.J.A., Archer, S. & Wilson, D.J.H. (1999). A comparison of the lichenometric and Schmidt hammer dating techniques based on data from the proglacial areas of some Icelandic glaciers. *Quaternary Science Reviews* **18** (1), 13–41.

Evans, D.J.A., Clark, C.D. & Rea, B.R. (2008). Landform and sediment imprints of fast glacier flow in the southwest Laurentide Ice Sheet. *Journal of Quaternary Science* **23** (3), 249–272.

Evans, D.J.A., Ewertowski, M. & Orton, C. (2015). Fláajökull (north lobe), Iceland: active temperate piedmont lobe glacial landsystem. *Journal of Maps* 1–13.

Evans, D.J.A. & Orton, C. (2015). Heinabergsjökull and Skalafellsjökull, Iceland: active temperate piedmont lobe and outwash head glacial landsystem. *Journal of Maps* **11** (3), 415–431.

Evans, D.J.A. & Rea, B.R. (1999). Geomorphology and sedimentology of surging glaciers: a land-systems approach. *Annals of Glaciology* **28** (1), 75–82.

Evans, D.J.A. & Rea, B.R. (2003). Surging glacier landsystem. In: D. J. A. Evans (ed.). *Glacial Landsystems*. 259–288, London: Hodder Arnold.

Evans, D.J.A., Rea, B.R., Hiemstra, J.F. & Ó Cofaigh, C. (2006). A critical assessment of subglacial mega-floods: a case study of glacial sediments and landforms in south-central Alberta, Canada. *Quaternary Science Reviews* **25** (13-14), 1638–1667.

Evans, D.J.A., Storrar, R.D. & Rea, B.R. (2016). Crevasse-squeeze ridge corridors: Diagnostic features of late-stage palaeo-ice stream activity. *Geomorphology* **258**, 40–50.

Evans, D.J.A. & Twigg, D.R. (2002). The active temperate glacial landsystem: a model based on Breiðamerkurjökull and Fjallsjökull, Iceland. *Quaternary Science Reviews* **21** (20-22), 2143–2177.

Evans, D.J.A., Young, N.J.P. & Ó Cofaigh, C. (2014). Glacial geomorphology of terrestrial-terminating fast flow lobes/ice stream margins in the southwest Laurentide Ice Sheet. *Geomorphology* **204**, 86–113.

Evenson, E.B., Burkhart, P.A., Gosse, J.C., Baker, G.S., Jackofsky, D., Meglioli, A., Dalziel, I., Kraus, S., Alley, R.B. & Berti, C. (2009). Enigmatic boulder trains, supraglacial rock avalanches, and the origin of ‘Darwin’s boulders,’ Tierra del Fuego. *GSA Today* **19** (12), 4–10.

Eyles, N. (1979). Facies of supraglacial sedimentation on Icelandic and Alpine temperate glaciers. *Canadian Journal of Earth Sciences* **16** (7), 1341–1361.

Glasser, N. & Jansson, K. (2008). The Glacial Map of southern South America. *Journal of Maps* **4** (1), 175–196.

Glasser, N.F. & Jansson, K.N. (2005). Fast-flowing outlet glaciers of the Last Glacial Maximum Patagonian Icefield. *Quaternary Research* **63** (2), 206–211.

Glasser, N.F., Jansson, K.N., Harrison, S. & Kleman, J. (2008). The glacial geomorphology and Pleistocene history of South America between 38 degrees S and 56 degrees S. *Quaternary Science Reviews* **27** (3-4), 365–390.

Glasser, N.F., Jansson, K.N., Harrison, S. & Rivera, A. (2005). Geomorphological evidence for variations of the North Patagonian Icefield during the Holocene. *Geomorphology* **71** (3-4), 263–277.

Hall, B.L., Porter, C.T., Denton, G.H., Lowell, T. V & Bromley, G.R.M. (2013). Extensive recession of Cordillera Darwin glaciers in southernmost South America during Heinrich Stadial 1. *Quaternary Science Reviews* **62** (0), 49–55.

Ham, N.R. & Attig, J.W. (1996). Ice wastage and landscape evolution along the southern margin of the Laurentide Ice Sheet, north-central Wisconsin. *Boreas* **25** (3), 171–186.

Harris, C., Williams, G., Brabham, P., Eaton, G. & McCarroll, D. (1997). Glaciotectonized quaternary sediments at Dinas Dinlle, Gwynedd, North Wales, and their bearing on the style of deglaciation in the Eastern Irish Sea. *Quaternary Science Reviews* **16** (1), 109–127.

Hein, A.S., Hulton, N.R.J., Dunai, T.J., Sugden, D.E., Kaplan, M.R. & Xu, S. (2010). The chronology of the Last Glacial Maximum and deglacial events in central Argentine Patagonia. *Quaternary Science Reviews* **29** (9-10), 1212–1227.

Hulton, N.R.J., Purves, R.S., McCulloch, R.D., Sugden, D.E. & Bentley, M.J. (2002). The Last Glacial Maximum and deglaciation in southern South America. *Quaternary Science Reviews* **21** (1-3), 233–241.

Johnson, M. & Clayton, L. (2003). Supraglacial landsystems in lowland terrain. In: D. J. A. Evans (ed.). *Glacial Landsystems*. 228–258, London: Hodder Arnold.

Kaplan, M.R., Coronato, A., Hulton, N.R.J., Rabassa, J.O., Kubik, P.W. & Freeman, S.P.H.T. (2007). Cosmogenic nuclide measurements in southernmost South America and implications for landscape change. *Geomorphology* **87** (4), 284–301.

Kaplan, M.R., Fogwill, C.J., Sugden, D.E., Hulton, N., Kubik, P.W. & Freeman, S.P.H.T. (2008a). Southern Patagonian glacial chronology for the Last Glacial period and implications for Southern Ocean climate. *Quaternary Science Reviews* **27** (3-4), 284–294.

Kaplan, M.R., Hein, A.S., Hubbard, A. & Lax, S.M. (2009). Can glacial erosion limit the extent of glaciation? *Geomorphology* **103** (2), 172–179.

Kaplan, M.R., Moreno, P.I. & Rojas, M. (2008b). Glacial dynamics in southernmost South America during Marine Isotope Stage 5e to the Younger Dryas chron: a brief review with a focus on cosmogenic nuclide measurements. *Journal of Quaternary Science* **23** (6-7), 649–658.

Kelley, S.E., Kaplan, M.R., Schaefer, J.M., Andersen, B.G., Barrell, D.J.A., Putnam, A.E., Denton, G.H., Schwartz, R., Finkel, R.C. & Doughty, A.M. (2014). High-precision 10Be chronology of moraines in the Southern Alps indicates synchronous cooling in Antarctica and New Zealand 42,000 years ago. *Earth and Planetary Science Letters* **405**, 194–206.

Kilian, R., Baeza, O., Ríos, F., Arz, H., Lamy, F., Witrz, J. & Baque, J. (2013). Evolución paleogeográfica y palaeoecológica del Sistema de fiordos del Seno Skyring y Seno Otway en la región de Magallanes durante el tardiglacial y Holoceno. *Anales del Instituto de la Patagonia*. [Online]. 41 (2) p.5–26.

Kilian, R. & Lamy, F. (2012). A review of Glacial and Holocene paleoclimate records from southernmost Patagonia (49–55°S). *Quaternary Science Reviews* **53** (0), 1–23.

Kilian, R., Schneider, C., Koch, J., Fesq-Martin, M., Biester, H., Casassa, G., Arévalo, M., Wendt, G., Baeza, O. & Behrmann, J. (2007). Palaeoecological constraints on late Glacial and Holocene ice retreat in the Southern Andes (53°S). *Global and Planetary Change* **59** (1–4), 49–66.

Kjaer, K.H. & Kruger, J. (2001). The final phase of dead-ice moraine development: processes and sediment architecture, Kotlujokull, Iceland. *Sedimentology* **48** (5), 935–952.

Kleman, J., Hättestrand, C., Stroeven, A.P., Jansson, K., De Angelis, H. & Borgström, I. (2006). Reconstruction of palaeo-ice sheets - inversion of their glacial geomorphological record. In: P. Knight (ed.). *Glaciology and Earth’s Changing Environment*. 192–198, Blackwell.

Krüger, J. (1994). Glacial processes, sediments, landforms and stratigraphy in the terminus region of Myrdalsjökull, Iceland. *Folia Geographica Danica* **21**, 1–233.

Lamy, F., Kaiser, J., Arz, H.W., Hebbeln, D., Ninnemann, U., Timm, O., Timmermann, A. & Toggweiler, J.R. (2007). Modulation of the bipolar seesaw in the Southeast Pacific during Termination 1. *Earth and Planetary Science Letters* **259** (3–4), 400–413.

Lovell, H., Fleming, E.J., Benn, D.I., Hubbard, B., Lukas, S., Rea, B.R., Noormets, R. & Flink, A.E. (2015). Debris entrainment and landform genesis during tidewater glacier surges. *Journal of Geophysical Research: Earth Surface* **120** (8), 1574–1595.

Lovell, H., Stokes, C.R. & Bentley, M.J. (2011). A glacial geomorphological map of the Seno Skyring-Seno Otway-Strait of Magellan region, southernmost Patagonia. *Journal of Maps* **7** (1), 318–339.

Lovell, H., Stokes, C.R., Bentley, M.J. & Benn, D.I. (2012). Evidence for rapid ice flow and proglacial lake evolution around the central Strait of Magellan region, southernmost Patagonia. *Journal of Quaternary Science* **27** (6), 625–638.

McCulloch, R.D. & Bentley, M.J. (1998). Late glacial ice advances in the Strait of Magellan, southern Chile. *Quaternary Science Reviews* **17** (8), 775–787.

McCulloch, R.D., Bentley, M.J., Tipping, R.M. & Clapperton, C.M. (2005a). Evidence for late-glacial ice dammed lakes in the central Strait of Magellan and Bahia Inutil, southernmost South America. *Geografiska Annaler Series a-Physical Geography* **87A** (2), 335–362.

McCulloch, R.D., Fogwill, C.J., Sugden, D.E., Bentley, M.J. & Kubik, P.W. (2005b). Chronology of the last glaciation in central Strait of Magellan and Bahia Inutil, southernmost South America. *Geografiska Annaler Series a-Physical Geography* **87A** (2), 289–312.

Meglioli, A. (1992). *Glacial Geology and Chronology of southernmost Patagonia and Tierra del Fuego, Argentina and Chile*. Lehigh University.

Mercer, J.H. (1976). Glacial history of southernmost South America. *Quaternary Research* **6** (2), 125–166.

Oldale, R.N. & O'Hara, C.J. (1984). Glaciotectonic origin of the Massachusetts coastal end moraines and a fluctuating late Wisconsinan ice margin. *Geological Society of America Bulletin* **95** (1), 61–74.

Peltier, W.R. (2004). Global glacial isostasy and the surface of the ice-age earth: The ICE-5G (VM2) Model and GRACE. *Annual Review of Earth and Planetary Sciences* **32** (1), 111–149.

Phillips, E., Lee, J.R. & Burke, H. (2008a). Progressive proglacial to subglacial deformation and syntectonic sedimentation at the margins of the Mid-Pleistocene British Ice Sheet: evidence from north Norfolk, UK. *Quaternary Science Reviews* **27** (19-20), 1848–1871.

Phillips, E.., Evans, D.J.. & Auton, C.. (2002). Polyphase deformation at an oscillating ice margin following the Loch Lomond Readvance, central Scotland, UK. *Sedimentary Geology* **149** (1-3), 157–182.

Phillips, W.M., Hall, A.M., Ballantyne, C.K., Binnie, S., Kubik, P.W. & Freeman, S. (2008b). Extent of the last ice sheet in northern Scotland tested with cosmogenic 10Be exposure ages. *Journal of Quaternary Science* **23** (2), 101–107.

Porter, S., Clapperton, C. & Sugden, D. (1992). Chronology and dynamics of deglaciation along and near the Strait of Magellan, southernmost South America. *SGU series Ca. Research paper*

Porter, S.C. (1990). Character and ages of Pleistocene Drifts in a transect across the Strait of Magellan. *Quaternary of South America and Antarctica Peninsula* **7**, 35–49.

Price, R. (1970). Moraines at Fjallsjökull, Iceland. *Arctic and Alpine Research* **2**, 27–42.

Putnam, A.E., Schaefer, J.M., Denton, G.H., Barrell, D.J.A., Birkel, S.D., Andersen, B.G., Kaplan, M.R., Finkel, R.C., Schwartz, R. & Doughty, A.M. (2013). The Last Glacial Maximum at 44°S documented by a 10Be moraine chronology at Lake Ohau, Southern Alps of New Zealand. *Quaternary Science Reviews* **62**, 114–141.

Rabassa, J. (2008). Late Cenozoic Glaciations in Patagonia and Tierra del Fuego. In: J. Rabassa (ed.). *Developments in Quaternary Sciences*. **11**, 151–204, Elsevier.

Rabassa, J., Coronato, A., Bujalesky, G., Salemme, M., Roig, C., Meglioli, A., Heusser, C., Gordillo, S., Roig, F., Borromei, A. & Quattrocchio, M. (2000). Quaternary of Tierra del Fuego, Southernmost South America: an updated review. *Quaternary International* **68-71** (0), 217–240.

Raedecke, L.D. (1978). Formas del terreno y depositos cuaternarios Tierra del Fuego central, Chile. *Revista geológica de Chile* **5**, 3–31.

Rotnicki, K. (1976). The theoretical basis for and a model of the origin of glaciotectonic deformations. *Quaestiones Geographicae* **3**, 103–139.

Rutter, N., Schnack, E.J., Rio, J. del, Fasano, J.L., Isla, F.I. & Radtke, U. (1989). Correlation and dating of Quaternary littoral zones along the Patagonian coast, Argentina. *Quaternary Science Reviews* **8** (3), 213–234.

Sagredo, E.A., Moreno, P.I., Villa-Martinez, R., Kaplan, M.R., Kubik, P.W. & Stern, C.R. (2011). Fluctuations of the Última Esperanza ice lobe (52°S), Chilean Patagonia, during the last glacial maximum and termination 1. *Geomorphology* **125** (1), 92–108.

Schaefer, J.M., Putnam, A.E., Denton, G.H., Kaplan, M.R., Birkel, S., Doughty, A.M., Kelley, S., Barrell, D.J.A.A., Finkel, R.C., Winckler, G., Anderson, R.F., Ninneman, U.S., Barker, S., Schwartz, R., Andersen, B.G. & Schluechter, C. (2015). The Southern Glacial Maximum 65,000 years ago and its Unfinished Termination. *Quaternary Science Reviews* **114**, 52–60.

Schomacker, A. (2008). What controls dead-ice melting under different climate conditions? A discussion. *Earth-Science Reviews* **90** (3–4), 103–113.

Schomacker, A., Benediktsson, Í.Ö. & Ingólfsson, Ó. (2014). The Eyjabakkajökull glacial landsystem, Iceland: Geomorphic impact of multiple surges. *Geomorphology* **218**, 98–107.

Sharp, M. (1985). 'Crevasse-Fill' Ridges: A Landform Type Characteristic of Surging Glaciers? *Geografiska Annaler, Series A: Physical Geography* **67** (3/4), 213–220.

Singer, B.S., Ackert, R.P. & Guillou, H. (2004). 40Ar/39Ar and K-Ar chronology of Pleistocene glaciations in Patagonia. *Geological Society of America Bulletin* **116** (3-4), 434–450.

Spedding, N. & Evans, D.J.. (2002). Sediments and landforms at Kvíárjökull, southeast Iceland: a reappraisal of the glaciated valley landsystem. *Sedimentary Geology* **149** (1-3), 21–42.

Stern, C.R., Moreno, P.I., Villa-Martínez, R., Sagredo, E.A., Prieto, A. & Labarca, R. (2011). Evolution of ice-dammed proglacial lakes in Última Esperanza, Chile: implications from the late-glacial R1 eruption of Reclús volcano, Andean Austral Volcanic Zone. *Andean geology* **38**, 82–97.

Stokes, C.R. & Clark, C.D. (2004). Evolution of late glacial ice-marginal lakes on the northwestern Canadian Shield and their influence on the location of the Dubawnt Lake palaeo-ice stream. *Palaeogeography, Palaeoclimatology, Palaeoecology* **215** (1-2), 155–171.

Stokes, C.R. & Clark, C.D. (1999). Geomorphological criteria for identifying Pleistocene ice streams. *Annals of Glaciology* **28** (1), 67–74.

Stokes, C.R. & Clark, C.D. (2001). Palaeo-ice streams. *Quaternary Science Reviews* **20** (13), 1437–1457.

Stokes, C.R., Spagnolo, M. & Clark, C.D. (2011). The composition and internal structure of drumlins: Complexity, commonality, and implications for a unifying theory of their formation. *Earth-Science Reviews* **107** (3-4), 398–422.

Storrar, R.D., Stokes, C.R. & Evans, D.J.A. (2014a). Increased channelization of subglacial drainage during deglaciation of the Laurentide Ice Sheet. *Geology* **42** (3), 239–242.

Storrar, R.D., Stokes, C.R. & Evans, D.J.A. (2014b). Morphometry and pattern of a large sample (>20,000) of Canadian eskers and implications for subglacial drainage beneath ice sheets. *Quaternary Science Reviews* **105**, 1–25.

Sugden, D.E., Bentley, M.J., Fogwill, C.J., Hulton, N.R.J., McCulloch, R.D. & Purves, R.S. (2005). Late-glacial glacier events in southernmost South America: A blend of ‘northern’and ‘southern’ hemispheric climatic signals? *Geografiska Annaler Series a-Physical Geography* **87A** (2), 273–288.

Teller, J.T. (2003). Subaquatic landsystems: large proglacial lakes. In: D. J. A. Evans (ed.). *Glacial Landsystems*. 348–371, London: Hodder Arnold.

van der Wateren, F. (1995). Structural geology and sedimentology of push moraines: processes of soft sediment deformation in a glacial environment and the distribution of. *Mededelingen Rijks Geologische Dienst* **54**.

Williams, G.D., Brabham, P.J., Eaton, G.P. & Harris, C. (2001). Late Devensian glaciotectonic deformation at St Bees, Cumbria: a critical wedge model. *Journal of the Geological Society* **158** (1), 125–135.

10 Figure captions

Figure 1. (A) Location of the study area in southern South America. (B) Overview of the geomorphological map from Darvill et al. (2014) showing the locations of figures and locations mentioned in the text. (C) Stylised representation of the southernmost part of the former Patagonian Ice Sheet, highlighting the five former ice lobes discussed in this paper. The approximate position of the ice divide is based on Hulton et al. (2002), but is shown for illustrative purposes only.

Figure 2. An overview of the glacial geomorphology relating to the Río Gallegos, Skyring, Otway and Magellan lobes, including key locations mentioned in the text (location shown in Figure 1).

Figure 3. (A) Overview of the glacial geomorphology associated with the centre of the BI-SSb lobe (location shown in Figure 1). Note the spillway marked by former shorelines associated with a proglacial lake that drained at Onaisín through Laguna Larga. (B) Enlargement of the central part of (A) showing cross-cutting relationships between subdued moraine topography and moraine ridges, glacial lineations and smaller hummocky terrain. (C) Enlargement of (B) showing the ordered nature of the regular hummocky terrain mini-ridges and the cross-cutting relationships more clearly.

Figure 4. (A) Overview of the glacial geomorphology associated with the Magellan lobe (location shown in Figure 1). Península Juan Mazía may have been the terminus of a surge-like advance (see text). (B) Enlargement of Punta Gente and the large field of elongate drumlins, in places draped by small moraine ridges.

Figure 5. Sketch log (A) and accompanying photographs (B and C) of proglacially tectonised lacustrine silts and sands within an end moraine of the BI-SSb lobe (location shown in Figure 3A). There is a high degree of folding and faulting. The large section suggests that the ice lobe retreated sufficiently for a sizeable proglacial lake to develop, prior to re-advance.

Figure 6. Sketch log (A) and accompanying photographs (B and C) of a glaciotectonised moraine associated with re-advance of the Otway lobe (location shown in Figure 2). The normal thrust faults are particularly highlighted by a deformed tephra layer in (C). The sediments are characteristic of outwash material that was likely deposited during retreat of the ice prior to re-advance and proglacial thrusting.

Figure 7. (A) A Google Earth image of larger irregular hummocky terrain from the south side of the BI-SSb lobe. (B) Field photograph of the hummocky topography on the north side of the BI-SSb lobe, illustrating the rounded hills and lakes. (C) A section through the inner band of larger hummocky terrain on the north side of the BI-SSb lobe. The top unit relates to this inner glacial limit (the San Sebastián drift), but overlies an earlier diamict unit and associated outwash (the Río Cullen drift), indicating that the ice lobe re-advanced (person for scale).

Figure 8. (A) A Google Earth image of regular hummocky terrain from the centre of the BI-SSb lobe (location shown in Figure 3B. This terrain resembles geometrical ridge networks and could be preserved crevasse-squeeze ridges. To illustrate this, (B) shows a Microsoft Bing Maps image of crevasse-squeeze ridges in front of the surging Brúarjökull glacier in

Iceland. Note that although the glaciers in question are markedly different in size, the images are at the same scale.

Figure 9. Glacial geomorphology found at the intersection between the Río Gallegos and Skyring lobes (location shown in Figure 2). (1) to (4) show a stylised formation mechanism for the irregular dissected ridge features. (1) The Río Gallegos advances first, creating a swath of drumlins (2), and possibly moraines, that are later overridden by an advance of the Skyring lobe (3). The order is dictated by the flow of meltwater from the Skyring lobe into the Río Gallegos basin (4).

Figure 10. Evidence for proglacial lakes within the study area. (A) shows the geomorphology and (B) the reconstructed ice limit and palaeo-Laguna Blanca proglacial lake just prior to drainage, when discharge flowed northwards. (C) The geomorphological evidence for lake drainage eastward into the Strait of Magellan once the Skyring lobe retreated beyond the bluff separating it from the Otway lobe (locations shown in Figure 2). (D) Raised shorelines, (E) laminated lake sediments with a dropstone circled, and (F) a drainage channel associated with palaeo-Laguna Blanca (locations shown in A and B). (G) Rhythmically laminated sediments from Laguna Verde (see Figure 4 for location). (H) Enlarged part of (G) showing several heavily deformed layers, possibly due to earthquake-induced tectonisation. (I) Dropstones are found within the Laguna Verde sequence (circled).

Figure 11. Glacial geomorphology of (A) the BI-SSb lobe and (B) the Río Gallegos, Skyring, Otway and Magellan lobes. The geomorphology has been grouped and re-coloured according to the three dominant landform suites indicative of an active temperate glacial landsystem.

Figure 12. (A) Simplified version of the glacial geomorphology in the study area to show the dominant ice flow and ice marginal features. (B) The flow-sets defined in this study (FS 1-20). (C) The dominant limits associated with four different sets of ice-marginal features. These were synthesised into glacial limits, shown in (D). The two innermost limits of the Skyring lobe are from Kilian et al. (2007). Eight of these limits are used in our glacial reconstruction time steps, coloured according to Figure 14.

Figure 13. Reconstructed glacial history for the five ice lobes studied, with eight time steps shown in (A) to (H). The hypothesised ice divide based on Hulton et al. (2002) is shown in (A) and (B) for reference. We show the rest of the ice sheet for completeness, with hypothesised gLGM limits based on Coronato et al. (2004). The rest of the ice sheet would have retreated over time, but that was not part of our study. Also shown in (A) and (B) are hypothesised drainage divides between the five ice lobes (bold dashed black lines) and the lines of topographic profiles for each ice lobe shown in Figure 14 (fine dashed black lines). Key flow-sets are shown and blue arrows show the direction of lake drainage routes. Question marks show where the ice configuration is unknown and black arrows in (H) show final retreat during time step 8. Published chronological data are shown where appropriate (see text for discussion). These are: argon dates (red text/circles); cosmogenic nuclide exposure dates (yellow circles) consisting of recalibrated ^{10}Be dates (black text), recalibrated ^{26}Al dates (italic blue text) and ^{36}Cl dates (italic green text); and cosmogenic nuclide depth profiles (bold black text/circles).

Figure 14. Topographic profiles for each ice lobe, shown as changes in elevation relating to present-day sea-level against distance from the hypothesised ice sheet divide. Ice flowed from left to right. The profiles from the ice divide to the outermost time step are shown in Figure 13A and B. The coloured numbers relate to the time steps shown in Figure 13D. Present-day sea-level is shown (short dashes), as well as the approximate sea-level at the gLGM (long dashes). Hence, the outermost limits of the BI-SSb lobe were in the Atlantic Ocean but would have formed on the exposed continental shelf. Also shown are the approximate heights of former proglacial lakes. The Río Gallegos lake would have dropped progressively over time, but the timing is not well constrained.

Figure 15. A distance-time graph for the five ice lobes over the last glacial cycle, based on cosmogenic nuclide and radiocarbon dating discussed in the text. Dated lava flows suggest that most of the ice lobes would have advanced during earlier glacial cycles (Meglioli, 1992; Singer et al., 2004; Kaplan et al., 2007). The BI-SSb lobe contains a large number of dates, but with scattered ages and large associated errors. It is not possible to reconcile the cosmogenic nuclide ages and some of the radiocarbon dates during deglaciation. The Magellan lobe contains fewer dates, but a more consistent ice-retreat history. The Otway and Skyring lobes contain few dates, but must have been retreating from a limit prior to *ca*. 30 ka because of the lake drainage from palaeo-Laguna Blanca in front of the Skyring, Otway and Magellan lobes (the blue stratigraphic correlation bar). Note the similarities in the glacial histories of these four ice lobes, including retreating from extensive positions prior to 30 ka and the gLGM, and rapid late-stage retreat. The timing of advance and retreat of the Río Gallegos lobe is not well constrained, partly because many of the cosmogenic nuclide and radiocarbon dates are from lateral positions that cannot be robustly linked to the former ice terminus. A large number of radiocarbon dates are shown from (Sagredo et al., 2011), but these cannot be tied to the ice terminus and are simply shown against the approximate ice distance in time step 7.

Table S1. Compilation of ^{10}Be and ^{26}Al cosmogenic nuclide exposure ages from the study area. Ages have been recalculated.

Table S2. Compilation of ^{36}Cl cosmogenic nuclide exposure ages from the study area. Ages have not been recalculated.

Table S3. Ages from two depth profiles through outwash associated with glacial limits in the study area. Ages are taken directly from Darvill et al. (2015b).

Table S4. Compilation of radiocarbon dates relating to glacier activity within the study area. Ages have been recalculated.

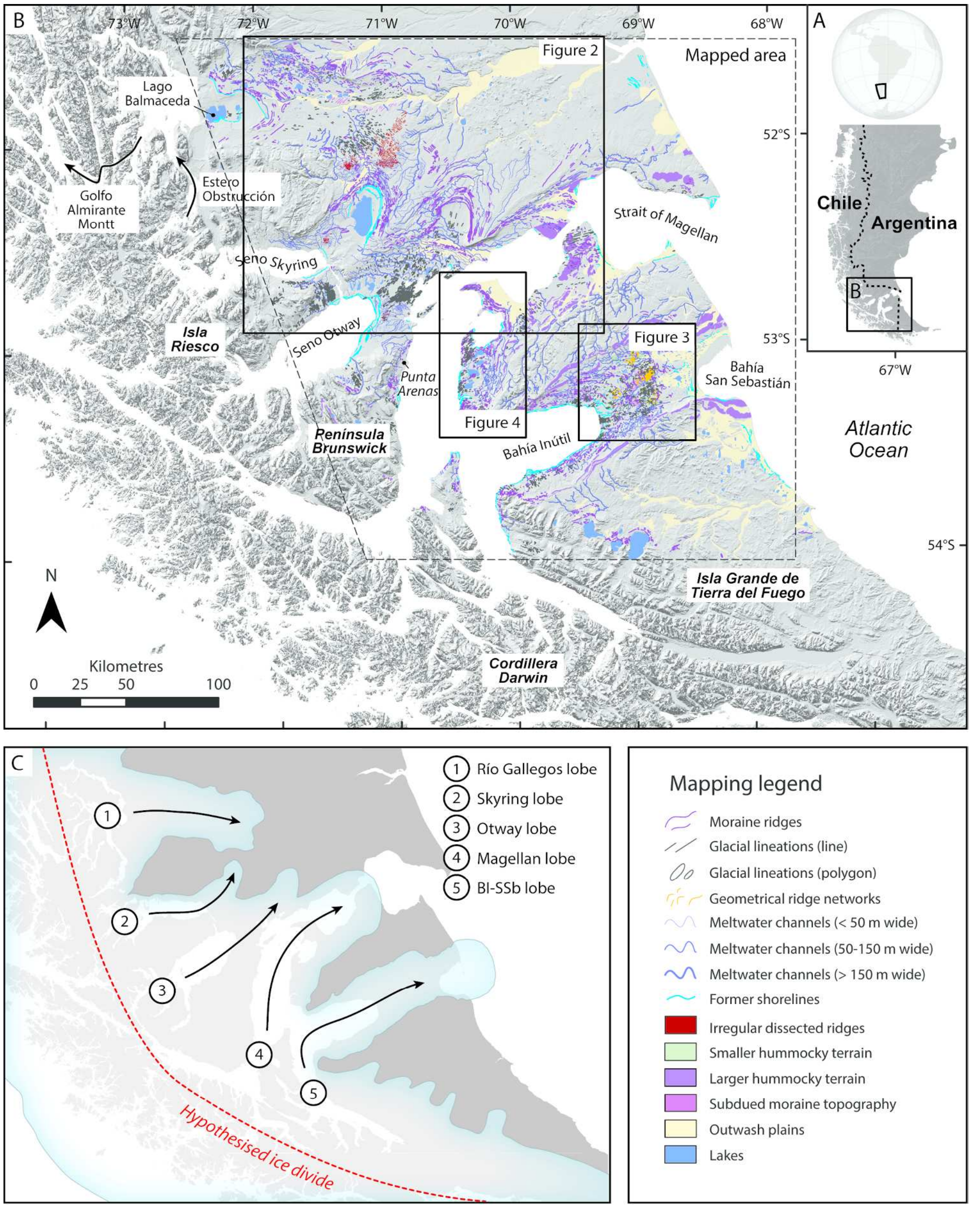

Figure 1. (A) Location of the study area in southern South America. (B) Overview of the geomorphological map from Darvill et al. (2014) showing the locations of figures and locations mentioned in the text. (C) Stylised representation of the southernmost part of the former Patagonian Ice Sheet, highlighting the five former ice lobes discussed in this paper. The approximate position of the ice divide is based on Hulton et al. (2002), but is shown for illustrative purposes only.
183x228mm (300 x 300 DPI)

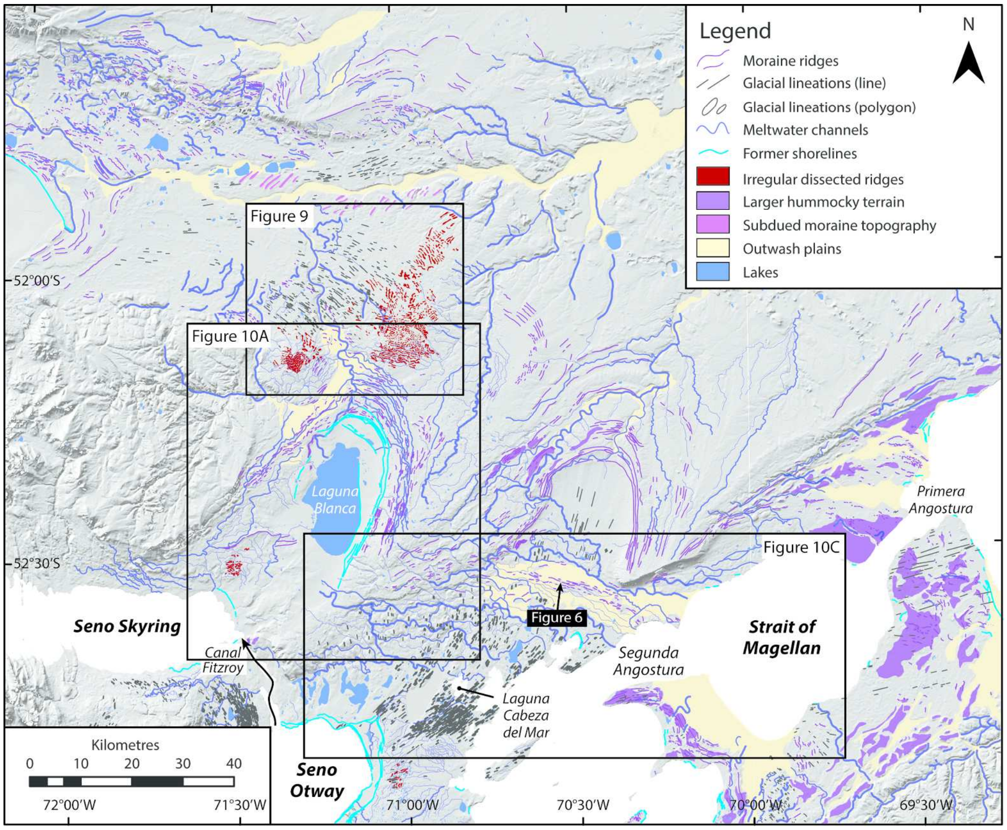

Figure 2. An overview of the glacial geomorphology relating to the Río Gallegos, Skyring, Otway and Magellan lobes, including key locations mentioned in the text (location shown in Figure 1).
184x151mm (300 x 300 DPI)

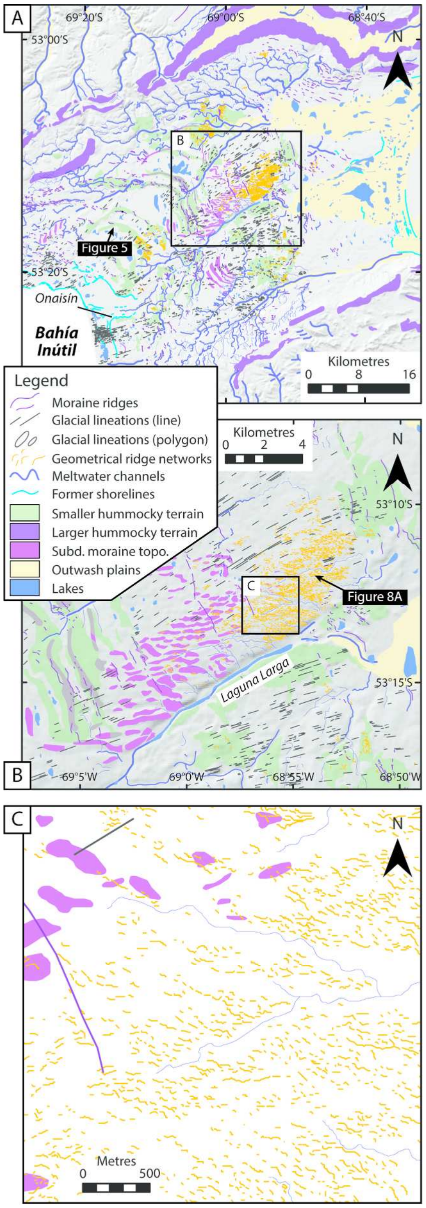

Figure 3. (A) Overview of the glacial geomorphology associated with the centre of the BI-SSb lobe (location shown in Figure 1). Note the spillway marked by former shorelines associated with a proglacial lake that drained at Onaisín through Laguna Larga. (B) Enlargement of the central part of (A) showing cross-cutting relationships between subdued moraine topography and moraine ridges, glacial lineations and smaller hummocky terrain. (C) Enlargement of (B) showing the ordered nature of the regular hummocky terrain mini-ridges and the cross-cutting relationships more clearly.
85x245mm (300 x 300 DPI)

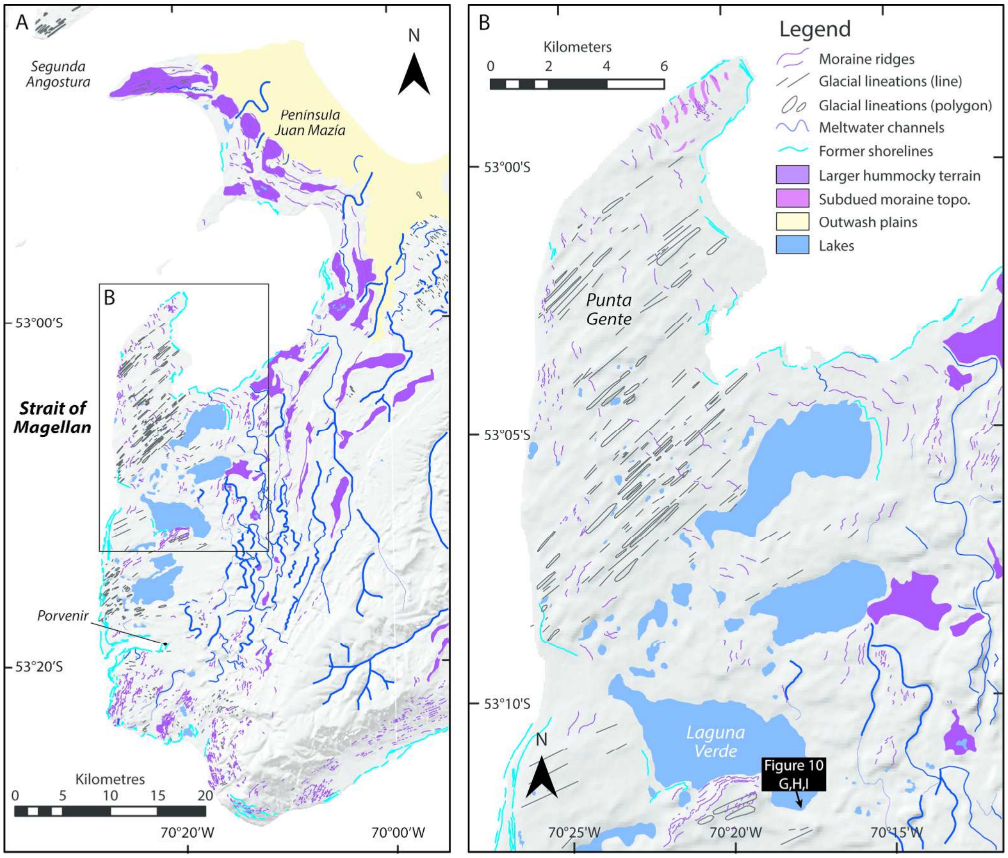

Figure 4. (A) Overview of the glacial geomorphology associated with the Magellan lobe (location shown in Figure 1). Península Juan Mazía may have been the terminus of a surge-like advance (see text). (B) Enlargement of Punta Gente and the large field of elongate drumlins, in places draped by small moraine ridges.

183x156mm (300 x 300 DPI)

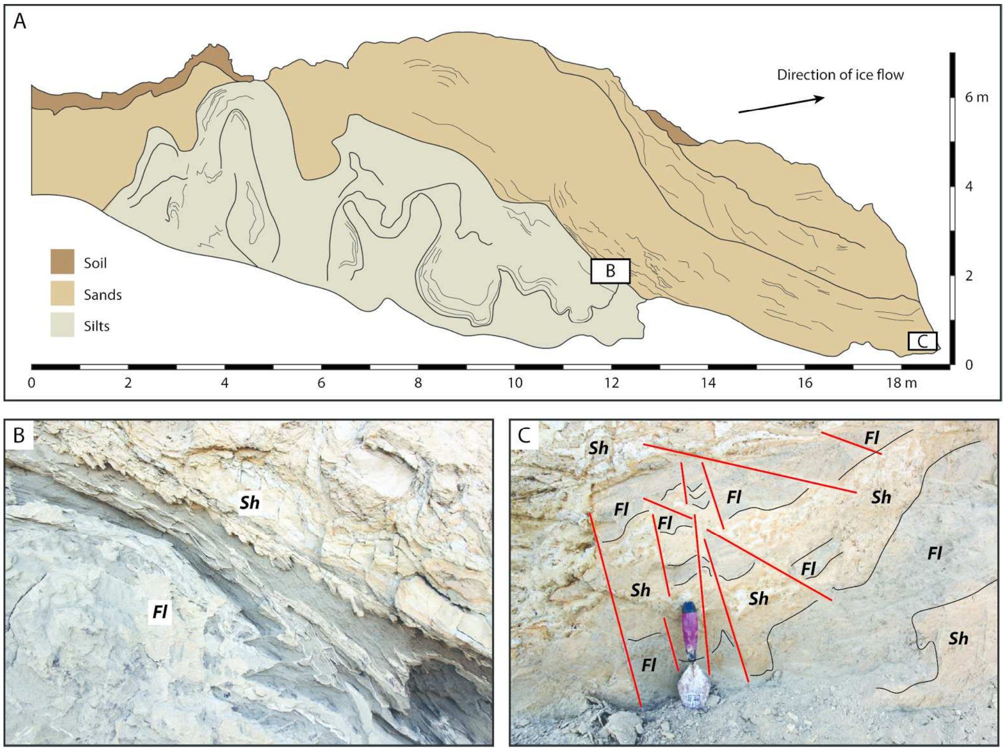

Figure 5. Sketch log (A) and accompanying photographs (B and C) of proglacially tectonised lacustrine silts and sands within an end moraine of the BI-SSb lobe (location shown in Figure 3A). There is a high degree of folding and faulting. The large section suggests that the ice lobe retreated sufficiently for a sizeable proglacial lake to develop, prior to re-advance.
183x136mm (300 x 300 DPI)

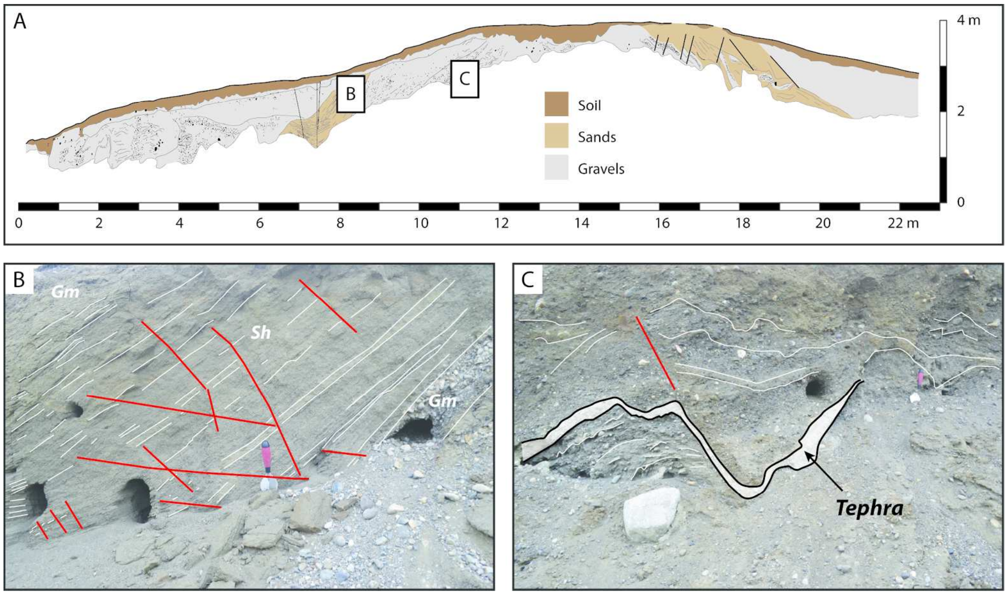

Figure 6. Sketch log (A) and accompanying photographs (B and C) of a glaciotectonised moraine associated with re-advance of the Otway lobe (location shown in Figure 2). The normal thrust faults are particularly highlighted by a deformed tephra layer in (C). The sediments are characteristic of outwash material that was likely deposited during retreat of the ice prior to re-advance and proglacial thrusting.
183x108mm (300 x 300 DPI)

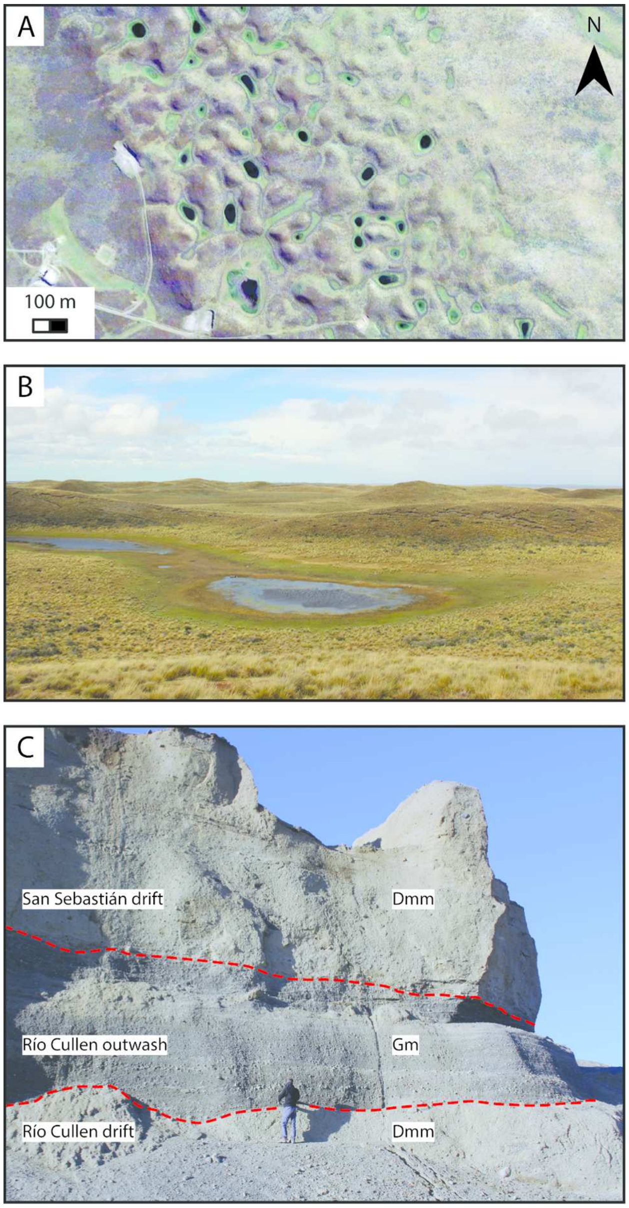

Figure 7. (A) A Google Earth image of larger irregular hummocky terrain from the south side of the BI-SSb lobe. (B) Field photograph of the hummocky topography on the north side of the BI-SSb lobe, illustrating the rounded hills and lakes. (C) A section through the inner band of larger hummocky terrain on the north side of the BI-SSb lobe. The top unit relates to this inner glacial limit (the San Sebastián drift), but overlies an earlier diamict unit and associated outwash (the Río Cullen drift), indicating that the ice lobe re-advanced (person for scale).
85x164mm (300 x 300 DPI)

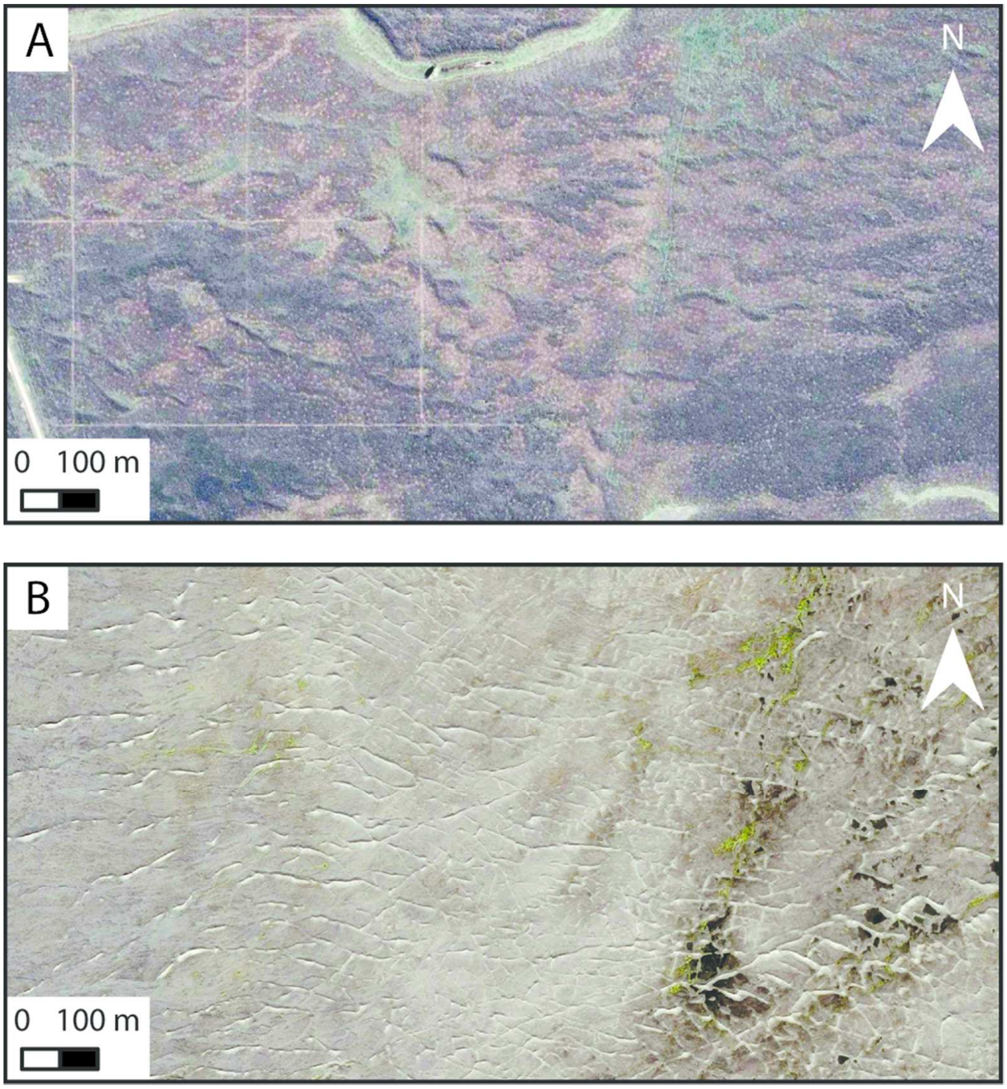

Figure 8. (A) A Google Earth image of regular hummocky terrain from the centre of the BI-SSb lobe (location shown in Figure 3B. This terrain resembles geometrical ridge networks and could be preserved crevasse-squeeze ridges. To illustrate this, (B) shows a Microsoft Bing Maps image of crevasse-squeeze ridges in front of the surging Brúarjökull glacier in Iceland. Note that although the glaciers in question are markedly different in size, the images are at the same scale.
85x92mm (300 x 300 DPI)

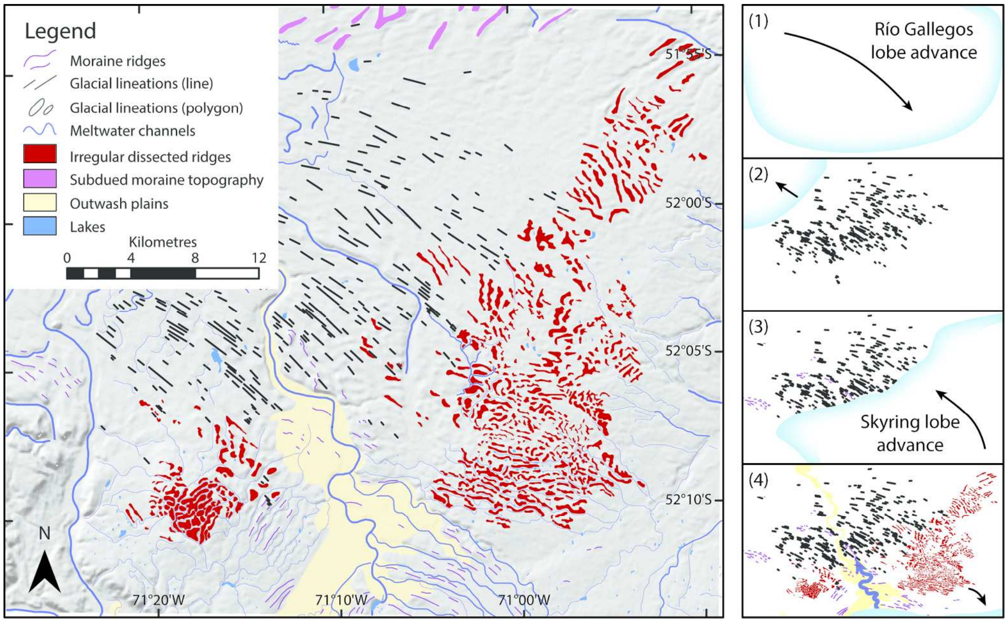

Figure 9. Glacial geomorphology found at the intersection between the Río Gallegos and Skyring lobes (location shown in Figure 2). (1) to (4) show a stylised formation mechanism for the irregular dissected ridge features. (1) The Río Gallegos advances first, creating a swath of drumlins (2), and possibly moraines, that are later overridden by an advance of the Skyring lobe (3). The order is dictated by the flow of meltwater from the Skyring lobe into the Río Gallegos basin (4).
183x112mm (300 x 300 DPI)

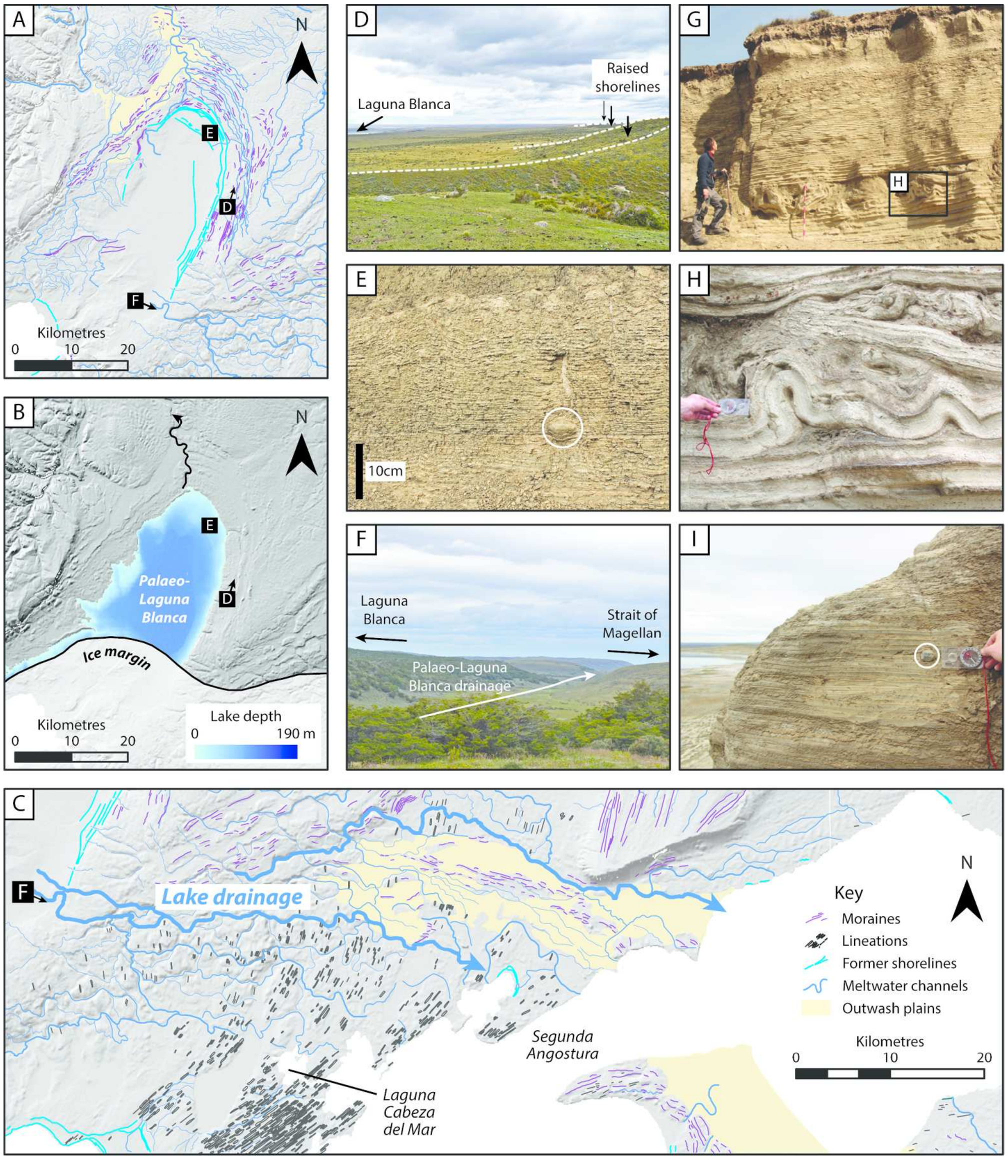

Figure 10. Evidence for proglacial lakes within the study area. (A) shows the geomorphology and (B) the reconstructed ice limit and palaeo-Laguna Blanca proglacial lake just prior to drainage, when discharge flowed northwards. (C) The geomorphological evidence for lake drainage eastward into the Strait of Magellan once the Skyring lobe retreated beyond the bluff separating it from the Otway lobe (locations shown in Figure 2). (D) Raised shorelines, (E) laminated lake sediments with a dropstone circled, and (F) a drainage channel associated with palaeo-Laguna Blanca (locations shown in A and B). (G) Rhythmically laminated sediments from Laguna Verde (see Figure 4 for location). (H) Enlarged part of (G) showing several heavily deformed layers, possibly due to earthquake-induced tectonisation. (I) Dropstones are found within the Laguna Verde sequence (circled).
183x212mm (300 x 300 DPI)

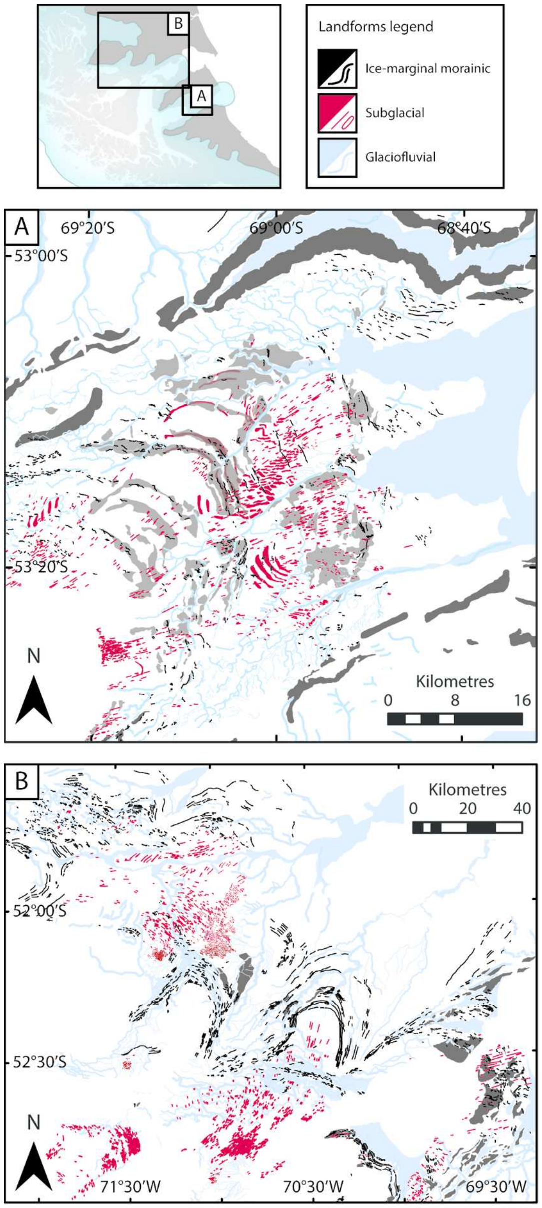

Figure 11. Glacial geomorphology of (A) the BI-SSb lobe and (B) the Río Gallegos, Skyring, Otway and Magellan lobes. The geomorphology has been grouped and re-coloured according to the three dominant landform suites indicative of an active temperate glacial landsystem.
85x191mm (300 x 300 DPI)

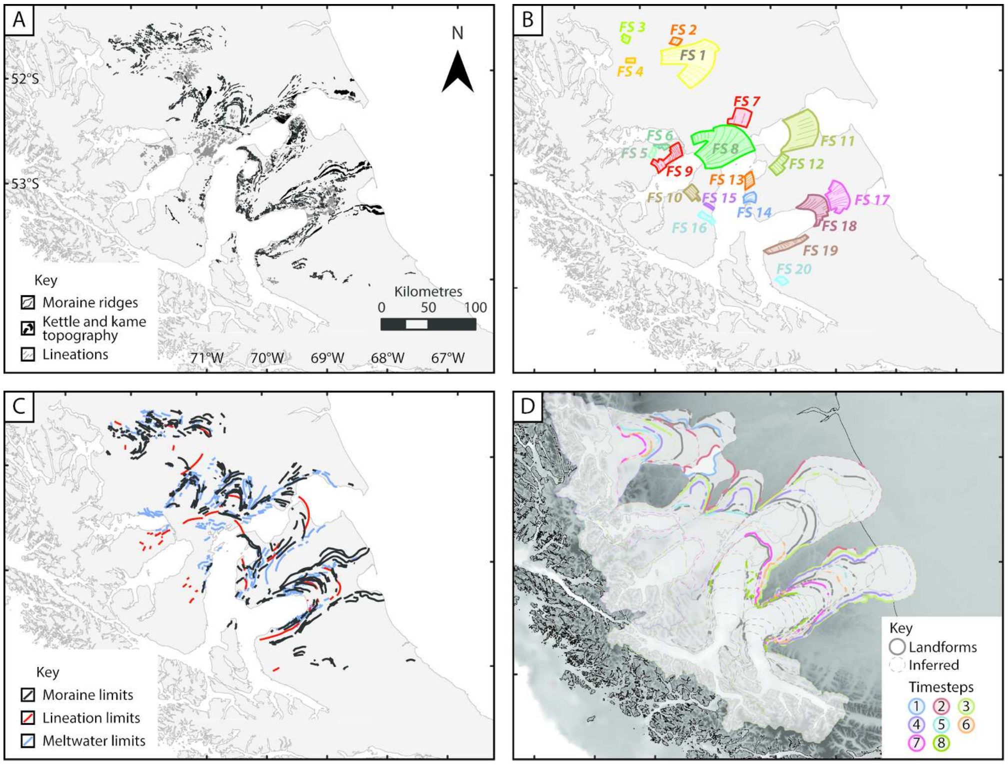

Figure 12. (A) Simplified version of the glacial geomorphology in the study area to show the dominant ice flow and ice marginal features. (B) The flow-sets defined in this study (FS 1-20). (C) The dominant limits associated with four different sets of ice-marginal features. These were synthesised into glacial limits, shown in (D). The two innermost limits of the Skyring lobe are from Kilian et al. (2007). Eight of these limits are used in our glacial reconstruction time steps, coloured according to Figure 14.
183x139mm (300 x 300 DPI)

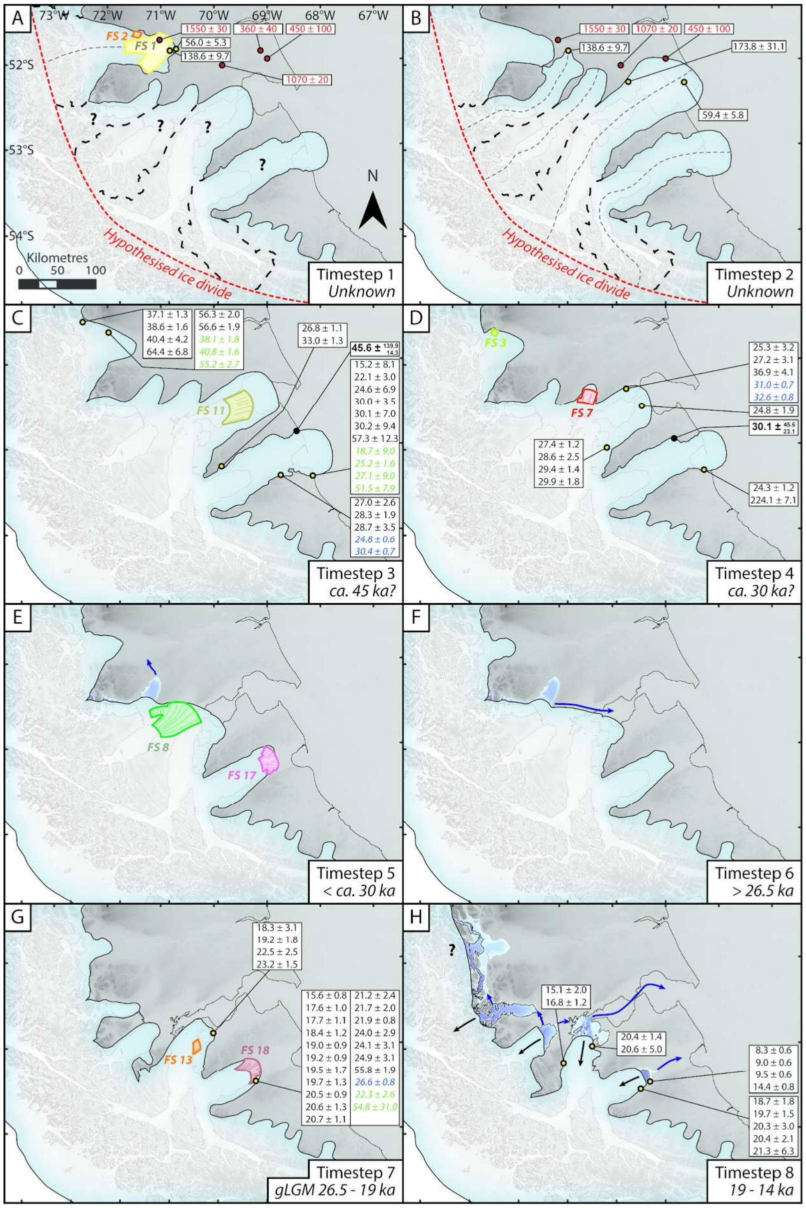

Figure 13. Reconstructed glacial history for the five ice lobes studied, with eight time steps shown in (A) to (H). The hypothesised ice divide based on Hulton et al. (2002) is shown in (A) and (B) for reference. We show the rest of the ice sheet for completeness, with hypothesised gLGM limits based on Coronato et al. (2004). The rest of the ice sheet would have retreated over time, but that was not part of our study. Also shown in (A) and (B) are hypothesised drainage divides between the five ice lobes (bold dashed black lines) and the lines of topographic profiles for each ice lobe shown in Figure 14 (fine dashed black lines). Key flow-sets are shown and blue arrows show the direction of lake drainage routes. Question marks show where the ice configuration is unknown and black arrows in (H) show final retreat during time step 8. Published chronological data are shown where appropriate (see text for discussion). These are: argon dates (red text/circles); cosmogenic nuclide exposure dates (yellow circles) consisting of recalibrated ^{10}Be dates (black text), recalibrated ^{26}Al dates (italic blue text) and ^{36}Cl dates (italic green text); and cosmogenic nuclide depth profiles (bold black text/circles).
163x245mm (300 x 300 DPI)

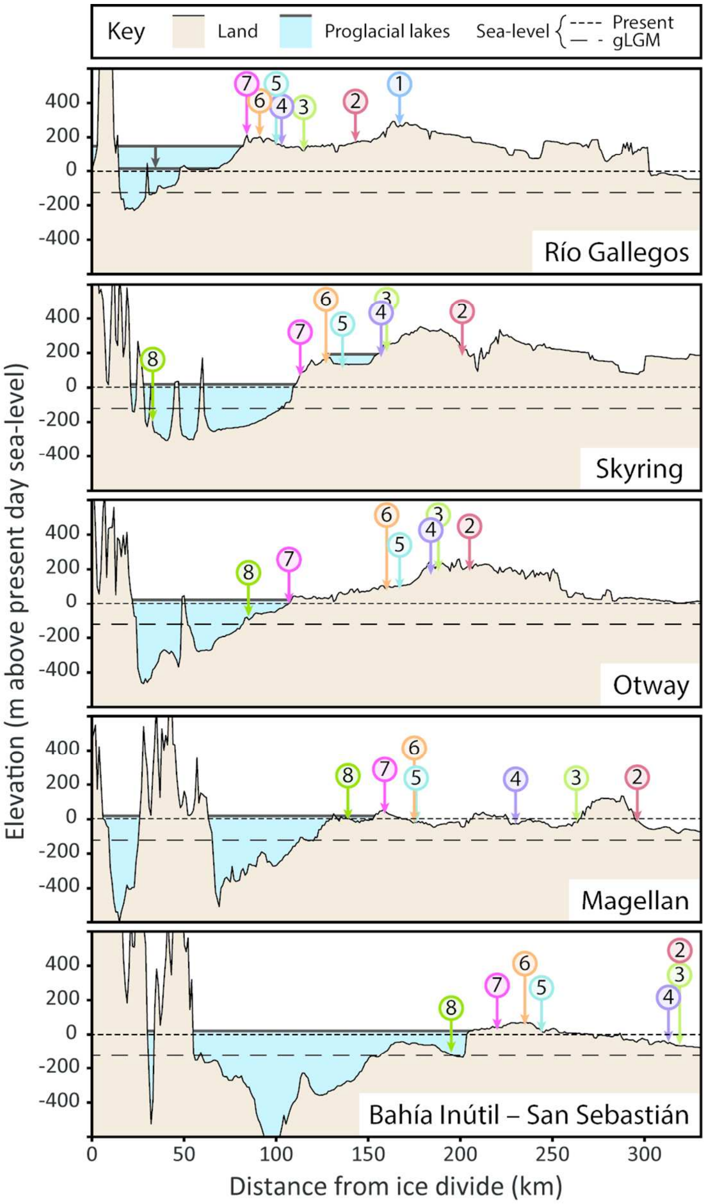

Figure 14. Topographic profiles for each ice lobe, shown as changes in elevation relating to present-day sea-level against distance from the hypothesised ice sheet divide. Ice flowed from left to right. The profiles from the ice divide to the outermost time step are shown in Figure 13A and B. The coloured numbers relate to the time steps shown in Figure 13D. Present-day sea-level is shown (short dashes), as well as the approximate sea-level at the gLGM (long dashes). Hence, the outermost limits of the BI-SSb lobe were in the Atlantic Ocean but would have formed on the exposed continental shelf. Also shown are the approximate heights of former proglacial lakes. The Río Gallegos lake would have dropped progressively over time, but the timing is not well constrained.
87x149mm (300 x 300 DPI)

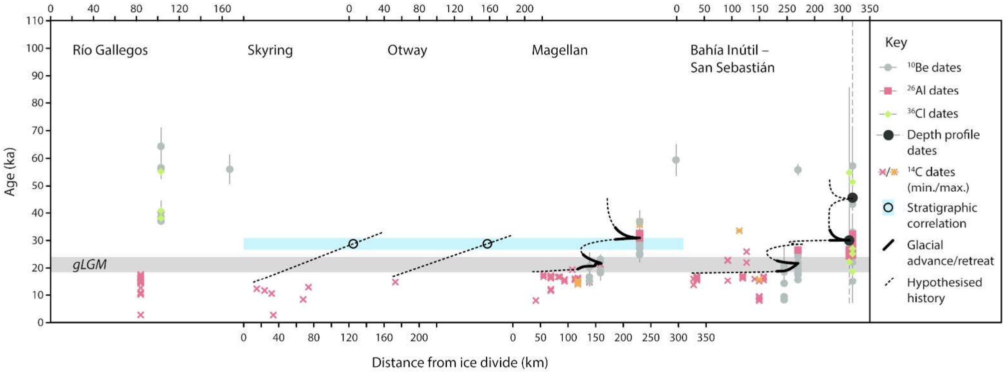

Figure 15. A distance-time graph for the five ice lobes over the last glacial cycle, based on cosmogenic nuclide and radiocarbon dating discussed in the text. Dated lava flows suggest that most of the ice lobes would have advanced during earlier glacial cycles (Meglioli, 1992; Singer et al., 2004; Kaplan et al., 2007). The BI-SSb lobe contains a large number of dates, but with scattered ages and large associated errors. It is not possible to reconcile the cosmogenic nuclide ages and some of the radiocarbon dates during deglaciation. The Magellan lobe contains fewer dates, but a more consistent ice-retreat history. The Otway and Skyring lobes contain few dates, but must have been retreating from a limit prior to ca. 30 ka because of the lake drainage from palaeo-Laguna Blanca in front of the Skyring, Otway and Magellan lobes (the blue stratigraphic correlation bar). Note the similarities in the glacial histories of these four ice lobes, including retreating from extensive positions prior to 30 ka and the gLGM, and rapid late-stage retreat. The timing of advance and retreat of the Río Gallegos lobe is not well constrained, partly because many of the cosmogenic nuclide and radiocarbon dates are from lateral positions that cannot be robustly linked to the former ice terminus. A large number of radiocarbon dates are shown from (Sagredo et al., 2011), but these cannot be tied to the ice terminus and are simply shown against the approximate ice distance in time step 7.
241x89mm (300 x 300 DPI)

Supplementary Information

Darvill et al. 'Dynamics of former ice lobes of the southernmost Patagonian Ice Sheet based on a glacial landsystems approach'

Contents

List of data tables

---

1 Age recalculation

In order to apply a broad chronological framework to the geomorphological reconstruction in this study, a large number of cosmogenic nuclide exposure ages and radiocarbon ages were compiled (Tables S1, S2, S3 and S4). The ^{10}Be, ^{26}Al and radiocarbon dates were also recalculated. There is an argument that recalculation may not be necessary because:

1. Uncertainty associated with cosmogenic nuclide exposure ages appears to be dominated by post-depositional effects (Kaplan et al., 2007; Evenson et al., 2009; Darvill et al., 2015a, 2015b) rather than uncertainties associated with age calculation.
2. Many of the landforms that have been exposure dated are older than the landforms used for regional or global ^{10}Be production rate calibrations (these are generally <20 ka; Borchers et al., 2016).

We recalculated ages because many of the original studies were published prior to updated calibration studies (both for cosmogenic nuclide exposure dating and radiocarbon dating). Moreover, whilst many of the ages may be older than the production rate datasets, this is still likely to be a better approximation of age than if older calibration datasets were used, and also creates consistency within our compilation, such that ages are compared on a similar scale. Overall, younger ages within the compilation (e.g. since the global Last Glacial Maximum) are changed little by this recalculation.

1.1 ^{10}Be and ^{26}Al exposure ages

A total of 75 ^{10}Be exposure ages and 13 ^{26}Al exposure ages were compiled for this study, shown in Table S1 (McCulloch et al., 2005b; Kaplan et al., 2007, 2008; Evenson et al., 2009; Darvill et al., 2015b; Sagredo et al., 2011). All exposure ages were recalculated using the CRONUS-earth online calculator version 2.2 (Wrapper script: 2.2; Main calculator: 2.1; Objective function: 2; Constants: 2.2.1; Muons: 1.1 (available at http://hess.ess.washington.edu/math/; see Balco et al., 2008). All calibration information was taken from the original studies, and a density of 2.7 g cm^{-3} was assumed where no density information was provided (reasonable given that all other published sample densities from the study area were either 2.65 g cm^{-3} or 2.7 g cm^{-3}). No erosion correction was applied so that the studies could be directly compared in a simple way, although in reality this is almost certainly unrealistic (Kaplan et al., 2007). The Macaulay River production rate from New Zealand was used (Putnam et al., 2010) because it overlaps at 1σ with a production rate from Lago Argentino in Patagonia (Kaplan et al., 2011) and has been used in other recent dating studies in Patagonia (Boex et al., 2013; Darvill et al., 2015b). The choice between these two production rates does not affect our discussion - the important point is that both production rates are lower than the global rate used in most of the original studies. Likewise, we consistently applied the 'Lm' time-dependent scaling scheme of Lal (1991) and Stone (2000), although the choice of scaling scheme makes little difference within the context of our discussion.

1.2 ^{36}Cl exposure ages

The details of nine ^{36}Cl exposure ages are compiled in Table S2 (Kaplan et al., 2007; Evenson et al., 2009). The dates were not recalculated given that progress in determining local ^{36}Cl production rates has not been made on the same scale as ^{10}Be production (and, by ratio scaling, ^{26}Al production). All ages were considered underestimates in the original studies due to postdepositional erosion and/or exhumation.

1.3 Depth profile exposure ages

Two exposure ages from depth profiles through outwash sediments related to glacial limits are compiled in Table S3, with all data from Darvill et al. (2015). These dates are modelled from numerous depth samples, and the reader is referred to the original study for full details of the modelling process and contextual discussion.

1.4 Radiocarbon ages

Data associated with 114 radiocarbon ages from the study area are compiled in Table S4 (Heusser et al., 1990; Clapperton et al., 1995; Anderson & Archer, 1999; Hall et al., 2013; McCulloch et al., 2005b, 2005a; McCulloch & Bentley, 1998; Uribe, 982; Heusser, 1987; Porter, 1990; Stern, 1992; McCulloch & Davies, 2001; Kilian et al., 2013; Sagredo et al., 2011). Where the raw ^{14}C ages and errors were available, dates were re-calibrated with CALIB 7.0 (Stuiver et al., 2005) using the INTCAL13 curve (Reimer, 2013). All dates were sorted according to their context as either minimum (MIN) or maximum (MAX) ages for glacier advances, or bracketed (M/M) where they dated material underlain and overlain by glacial sediments.

2.1	2.7	1	0	170000	20100	S555	1109800	9400	KNSTD	Yes	Boulder	28695	3473	30396	712
2.4	2.7	1	0	167000	10300	S555	904100	9000	KNSTD	Yes	Boulder	28256	1858	24762	593
2.5	2.7	1	0	109000	12200	S555	0	0	KNSTD		Boulder	21223	2432		
2.5	2.7	1	0	90400	4650	NIST_30600	0	0	KNSTD		Boulder	17597	985		
1.4	2.7	1	0	107000	5430	NIST_30600	849400	18500	KNSTD		Boulder	20662	1144	26583	824
1	2.7	1	0	100000	4270	NIST_30600	0	0	KNSTD		Boulder	19020	913		
0.5	2.7	1	0	219739	7456	S555	0	0	KNSTD		Boulder	33039	1338		
0.5	2.7	1	0	177837	5957	S555	0	0	KNSTD		Boulder	26762	1072		
0.9	2.7	1	0	125930	10467	S555	0	0	KNSTD		Boulder	19520	1684		
0.6	2.7	1	0	107975	31430	S555	0	0	KNSTD		Boulder	21346	6264		
2.9	2.7	1	0	92397	8565	S555	0	0	KNSTD		Boulder	18670	1785		
2	2.65	1	0	101010	6427	KNSTD	0	0	KNSTD		Boulder	18401	1241		
2	2.65	1	0	112971	6525	KNSTD	0	0	KNSTD		Boulder	20590	1275		
2	2.65	1	0	98689	5883	KNSTD	0	0	KNSTD		Boulder	17717	1128		
2	2.65	1	0	106896	4586	KNSTD	0	0	KNSTD		Boulder	19197	925		
1	2.65	1	0	123064	3493	KNSTD	0	0	KNSTD		Boulder	21938	785		
4	2.65	1	0	303471	7871	KNSTD	0	0	KNSTD		Boulder	55846	1907		
2	2.65	1	0	111186	4324	KNSTD	0	0	KNSTD		Boulder	20462	914		
6	2.65	1	0	82817	4082	KNSTD	0	0	KNSTD		Boulder	15638	844		
5	2.65	1	0	104681	6420	KNSTD	0	0	KNSTD		Boulder	19725	1288		
3	2.65	1	0	42024	2657	KNSTD	0	0	KNSTD		Boulder	8327	557		
3	2.65	1	0	47831	2825	KNSTD	0	0	KNSTD		Boulder	9480	597		
2	2.65	1	0	45843	3122	KNSTD	0	0	KNSTD		Boulder	9013	645		
2	2.65	1	0	72529	3798	KNSTD	0	0	KNSTD		Boulder	14350	815		
6	2.7	0.999999	0	130107	3377	NIST_27900	918950	33591	Z92-0222		Outwash	31022	1053	32404	1396
6	2.7	0.999999	0	180591	4619	NIST_27900	868057	29274	Z92-0222	Yes	Outwash	43215	1459	30580	1241
6	2.7	0.999999	0	99630	2922	NIST_27900	784025	27306	Z92-0222		Outwash	23704	867	27575	1144
6	2.7	0.999999	0	112414	3101	NIST_27900	806137	29141	Z92-0222		Outwash	26770	942	28365	1210
6	2.7	0.999999	0	127390	3653	NIST_27900	856986	29261	Z92-0222		Outwash	26633	961	26470	1082
6	2.7	0.999999	0	118438	4222	NIST_27900	792773	35652	Z92-0222		Outwash	24750	1036	24463	1234
6	2.7	0.999999	0	131073	5696	NIST_27900	819874	26226	Z92-0222		Outwash	27408	1338	25309	987
6	2.7	0.999999	0	118430	4081	NIST_27900	860572	36911	Z92-0222		Outwash	24749	1011	26582	1292
4	2.7	1	0	148976	8492	S555	0	0	KNSTD		Boulder	29898	1835		
4	2.7	1	0	145383	12358	S555	0	0	KNSTD		Boulder	28647	2530		
4	2.7	1	0	135386	4874	S555	0	0	KNSTD		Boulder	27394	1156		
1.5	2.7	1	0	930000	158000	S555	0	0	KNSTD		Boulder	173758	31085		
2.6	2.7	1	0	127000	9490	S555	0	0	KNSTD	Yes	Boulder	24818	1942		
1	2.7	1	0	286000	26900	S555	0	0	KNSTD	Yes	Boulder	59402	5817		
0.5	2.7	1	0	130000	16200	S555	0	0	KNSTD	Yes	Boulder	25275	3216		
1.5	2.7	1	0	143000	16100	S555	1004400	6800	KNSTD	Yes	Boulder	27162	3135	30958	708
0.9	2.7	1	0	189000	20600	S555	1032900	9600	KNSTD	Yes	Boulder	36878	4135	32647	776

Table S2. Compilation of ^{36}Cl cosmogenic nuclide exposure ages from the study area. Ages have not been recalculated.

Author	Year	Glacial system	Moraine system	Time step	Sample name	Latitude (DD)	Longitude (DD)	Outliers?	Sample type	Cl-36 age (years)	Cl-36 error (years)
Kaplan	2007	Bahía Inútil	Rio Cullen	3	RC-04-01	-53.47	-68.321	Yes	Boulder	51500	7900
Kaplan	2007	Bahía Inútil	Rio Cullen	3	RC-04-04f	-53.504	-68.155	Yes	Boulder	25200	1600
Kaplan	2007	Bahía Inútil	B limit	4	TF-04-04	-53.607	-69.233	Yes	Boulder	54800	31000
Kaplan	2007	Bahía Inútil	B limit	4	TF-04-05	-53.605	-69.282	Yes	Boulder	22300	2600
Evenson	2009	Bahía Inútil	Rio Cullen	3	ARG-00-Tdf-039	-	-	Yes	Boulder	18700	9000
Evenson	2009	Bahía Inútil	Rio Cullen	3	ARG-00-Tdf-043	-	-	Yes	Boulder	27100	9000
Evenson	2009	Rio Gallegos	Bella Vista	3	CRG-T32-99-23	-51.69	-72	Yes	Boulder	55200	2700
Evenson	2009	Rio Gallegos	Bella Vista	3	CRG-T41-99-25	-51.69	-72	Yes	Boulder	40800	1600
Evenson	2009	Rio Gallegos	Bella Vista	3	CRG-T41-99-26	-51.69	-72	Yes	Boulder	38100	1800

Table S3. Ages from two depth profiles through outwash associated with glacial limits in the study area. Ages are taken directly from Darvill et al. (2015b).

Author	Year	Glacial system	Moraine system	Time step	Sample name	Latitude (DD)	Longitude (DD)	Outliers?	Sample type	Depth profile age (years)	Depth profile positive error (years)	Depth profile negative error (years)
Darvill	2015b	Bahía Inútil	Rio Cullen outwash	3	Cullen profile	-52.8899	-68.4244		Depth profile	45600	139900	14300
Darvill	2015b	Bahía Inútil	San Sebastian outwash	4	Filaret profile	-52.9743	-68.831		Depth profile	30100	45600	23100

pilation of radiocarbon dates relating to glacier activity within the study area. Ages have been recalculated.

Year	Glacial system	Site	Time step	Sample name	Latitude (DD)	Longitude (DD)	14C date	± 1σ	Calib age	Calib error
1990	Bahía Inútil	Chorillo Rosario	8	QL-1683	-53.4476	-70.0901	13280	80	15974	247
1990	Bahía Inútil	Chorillo Rosario	8	QL-4293	-53.4476	-70.0901	12010	80	13868	235
1990	Bahía Inútil	Chorillo Rosario	8	QL-4294	-53.4476	-70.0901	12060	80	13932	187
1995	Bahía Inútil	Punta Cameron	8	A-6791	-53.6871	-69.9249	13030	260	15556	850
1995	Bahía Inútil	Puente Charlie	8	A-7569	-53.4294	-70.053	12740	120	15156	485
1995	Bahía Inútil	Puente Charlie	8	A-7570	-53.4294	-70.053	7240	70	8063	122
1995	Bahía Inútil	Isla Dawson East	4	AA-10414	-53.6333	-70.4667	29500	380	33609	775
1999	Bahía Inútil	V17-70	8	CAMS-22179	-53.5667	-70.3	21740	120	25989	226
1999	Bahía Inútil	V17-83	8	CAMS-22180	-53.8667	-70.3667	19050	90	22950	330
1999	Bahía Inútil	V17-83	8	OS-2164	-53.8667	-70.3667	12850	60	15362	226
1999	Bahía Inútil	V17-83	8	OS-2165	-53.8667	-70.3667	18900	80	22757	244
1999	Bahía Inútil	V17-70	8	OS-2166	-53.5667	-70.3	18150	100	22024	294
2013	Bahía Inútil	Punta Marinelli Bog	8	OS-61545	-54.3412	-69.5313	14050	70	17084	290
2013	Bahía Inútil	Punta Marinelli Bog	8	OS-61550	-54.3412	-69.5313	12950	60	15490	235
2013	Bahía Inútil	Punta Esperanza	8	OS-61551	-54.3119	-69.949	13350	65	16049	216
2013	Bahía Inútil	Punta Marinelli Bog	8	OS-61606	-54.3412	-69.5313	13400	85	16108	272
2013	Bahía Inútil	Punta Marinelli Bog	8	OS-63929	-54.3412	-69.5313	13250	55	15927	197
2013	Bahía Inútil	Punta Marinelli Bog	8	OS-64068	-54.3412	-69.5313	13250	85	15937	264
2013	Bahía Inútil	Punta Marinelli Bog	8	OS-64070	-54.3412	-69.5313	13650	90	16496	313
2013	Bahía Inútil	Punta Marinelli Bog	8	OS-64095	-54.3412	-69.5313	13950	55	16896	250
2013	Bahía Inútil	Punta Esperanza	8	OS-64245	-54.3119	-69.949	11900	190	13778	468
2005a	Bahía Inútil	Puente Charlie	8	AA-35087	-53.4294	-70.053	8320	65	9303	173
2005a	Bahía Inútil	Estancia Cameron II	8	AA-42413	-53.6366	-69.6492	13980	120	16968	412
2005a	Bahía Inútil	Estancia California	8	AA-42414	-53.5957	-69.5605	13614	86	16445	300
2005a	Bahía Inútil	Puente Charlie	8	Beta-117945	-53.4294	-70.053	8230	70	9214	192
2005a	Bahía Inútil	Puente Charlie	8	SRR-6286	-53.4294	-70.053	8545	45	9514	47
2005a	Bahía Inútil	Puente Charlie	8	SRR-6287	-53.4294	-70.053	10875	45	12755	61
2005a	Bahía Inútil	Puente Charlie	8	SRR-6288	-53.4294	-70.053	13160	45	15824	191
2005a	Bahía Inútil	Puente Charlie	8	SRR-6496	-53.4294	-70.053	13205	55	15877	197
2005a	Bahía Inútil	Puente Charlie	8	SRR-6497	-53.4294	-70.053	12960	55	15500	226
2005a	Bahía Inútil	Puente Charlie	8	SRR-6498	-53.4294	-70.053	13125	55	15762	240
2005a	Bahía Inútil	Puente Charlie	8	SRR-6499	-53.4294	-70.053	10830	50	12738	61
2005a	Bahía Inútil	Puente Charlie	8	SRR-6500	-53.4294	-70.053	7660	50	8465	83
1995	Bahía Inútil/Magellan	Estancia Esmerelda II	8	A-6793	-53.584	-70.5041	14260	350	17284	929
1995	Bahía Inútil/Magellan	Estancia Esmerelda I	8	A-6807	-53.5917	-70.4648	13425	310	16185	915
1995	Bahía Inútil/Magellan	Estancia Esmerelda II	8	A-6814	-53.584	-70.5041	13650	310	16556	895
1998	Bahía Inútil/Magellan	Estancia Esmerelda II	8	SSR-5143	-53.584	-70.5041	13890	50	16812	233
2013	Cordillera Darwin	Caleta Olla 2	-	OS-61542	-54.9377	-69.1722	10300	50	12111	275
2013	Cordillera Darwin	BL-07-15	-	OS-61603	-54.8176	-69.735	9310	65	10486.5	195.5
2013	Cordillera Darwin	Ventisquero Holanda 1	-	OS-61638	-54.9441	-69.1317	12550	60	14785.5	355.5
2013	Cordillera Darwin	BL-07-16B	-	OS-64237	-54.8235	-69.7364	12350	120	14508.5	492.5
1982	Magellan	Pampa Alegre	8	DIC-2322	-53.0709	-70.8725	11940	110	13813	268
1987	Magellan	Puerto del Hambre	8	AA-30651	-53.6177	-70.9519	14455	115	17617	317
1987	Magellan	Punta Arenas	8	QL-1470	-53.1383	-70.8973	13400	140	16140	415
1990	Magellan	Parque Chacabunco	7	QL-1650	-53.0333	-70.8333	47000	>	Out of range	-
1990	Magellan	Cabo Porpesse	3	QL-1660	-52.95	-70.7833	42400	2500/3700	Out of range	-
1992	Magellan	Pampa Alegre	8	np	-53.0709	-70.8725	11795	365	13994	1006

1995	Magellan	Rio Tres Brazos	4	AA-10412	-53.2667	-70.9167	43945	2100	Out of range	-
1995	Magellan	Rio Tres Brazos	4	AA-10413	-53.2667	-70.9167	43810	2120	Out of range	-
1995	Magellan	Estancia Amarillo	8	AA-12872	-53.4036	-70.9863	13945	105	16895	378
1995	Magellan	Rio Tres Brazos	4	AA12875	-53.2667	-70.9167	41900	1700	Out of range	-
1995	Magellan	Rio Tres Brazos	4	AA12875	-53.2667	-70.9167	27690	335	31770	736
1995	Magellan	Rio Tres Brazos	4	AA-8396	-53.2667	-70.9167	47200	>	Out of range	-
1995	Magellan	Pampa Alegre	8	SRR-4583	-53.0709	-70.8725	12070	45	13920	150
1998	Magellan	Cabo Valentin II	8	A-8164	-53.5686	-70.5311	10055	65	11619	328
1998	Magellan	14C Age estimate for Reclus tephra layer	8	AA-20570	-53.6177	-70.9519	12840	100	15377	331
2011	Magellan	Puerto del Hambre	8	CAMS-65903	-53.6177	-70.9519	14470	50	17659	198
2005b	Magellan	Rio Tres Brazos	4	AA-30863	-53.2667	-70.9167	40800	1300	Out of range	-
2005b	Magellan	Rio Tres Brazos	4	AA-30864	-53.2667	-70.9167	41100	1500	Out of range	-
2005b	Magellan	Porvenir 2 kettle hole within terrace	8	AA-30913	-53.3	-70.3333	16090	100	19403	288
2005b	Magellan	14C Age estimate for Reclus tephra layer	8	AA-30918	-53.1383	-70.8973	12525	75	14713	407
2005b	Magellan	Porvenir 2 kettle hole within terrace	7	Beta-117944	-53.3	-70.3333	16130	60	19448	200
2005a	Magellan	Pampa Alegre	8	A-6818	-53.0709	-70.8725	11805	220/215	13642	83
2005a	Magellan	Cabo Valentin II	8	AA-23077	-53.5686	-70.5311	10314	81	12160	355
2005a	Magellan	Bahia Lomas	8	AA-30917	-53.7928	-70.6725	7250	55	8072	102
2005a	Magellan	Punta Arenas	8	AA-30919	-53.1383	-70.8973	13050	95	15620	325
2005a	Magellan	San Felipe	8	AA-35082	-53.6042	-70.9641	13850	90	16753	323
2005a	Magellan	Estancia Guairabo	8	AA-42415	-53.3111	-70.9476	13186	78	15842	268
2005a	Magellan	Estancia Amarillo	8	AA-42416	-53.4036	-70.9863	13849	81	16753	302
2005a	Magellan	Pampa Alegre	8	Beta-117943	-53.0709	-70.8725	12820	100	15342	348
2005a	Magellan	Pampa Alegre	8	SRR-6501	-53.0709	-70.8725	12720	55	15125	210
2005a	Magellan	Pampa Alegre	8	SRR-6502	-53.0709	-70.8725	13155	60	15808	231
2005a	Magellan	Pampa Alegre	8	SSR-6502	-53.0709	-70.8725	13155	60	15808	231
2013	Otway	OTW2	8	-	-52.9663	-72.0214	-	-	14780	-
2011	Rio Gallegos	Eberhardt	7	CAMS 107008	-51.5779	-72.6684	13745	50	16611.5	252.5
2011	Rio Gallegos	Eberhardt	7	CAMS 107052	-51.5779	-72.6684	10695	40	12647.5	69.5
2011	Rio Gallegos	Lago Dorotea	7	CAMS 107053	-51.5336	-72.4829	12670	45	15045.5	213.5
2011	Rio Gallegos	Lago Dorotea	7	CAMS 107054	-51.5336	-72.4829	12460	90	14625.5	434.5
2011	Rio Gallegos	Lago Dorotea	7	CAMS 107055	-51.5336	-72.4829	13000	60	15542	241
2011	Rio Gallegos	Lago Dorotea	7	CAMS 107092	-51.5336	-72.4829	14170	45	17264.5	192.5
2011	Rio Gallegos	Vega Benitez	7	CAMS 107093	-51.5582	-72.5828	14520	140	17674	355
2011	Rio Gallegos	Lago Dorotea	7	CAMS 114975	-51.5336	-72.4829	14105	45	17178.5	212.5
2011	Rio Gallegos	Vega Benitez	7	CAMS 115804	-51.5582	-72.5828	12580	35	14921.5	209.5
2011	Rio Gallegos	Pantano Dumestre	7	CAMS 125918	-51.8053	-72.4356	12910	25	15425.5	171.5
2011	Rio Gallegos	Pantano Laurita	7	CAMS 128971	-51.6788	-72.2741	9570	40	10919	182
2011	Rio Gallegos	Pantano Laurita	7	CAMS 128972	-51.6788	-72.2741	2720	35	2817	62
2011	Rio Gallegos	Pantano Laurita	7	CAMS 128973	-51.6788	-72.2741	9495	35	10836.5	232.5
2011	Rio Gallegos	Lago Arauco	7	CAMS 128974	-51.9663	-72.0434	13330	70	16027.5	226.5
2011	Rio Gallegos	Lago Arauco	7	CAMS 128975	-51.9663	-72.0434	13245	50	15921	186
2011	Rio Gallegos	Lago Arauco	7	CAMS 128976	-51.9663	-72.0434	12500	60	14686	385
2011	Rio Gallegos	Lago Pintito	7	CAMS 128980	-52.0445	-72.3808	13670	50	16501.5	236.5
2011	Rio Gallegos	Lago Pintito	7	CAMS 128981	-52.0445	-72.3808	13610	50	16417.5	212.5
2011	Rio Gallegos	Pantano Dumestre	7	CAMS 129005	-51.8053	-72.4356	12875	45	15387	202
2011	Rio Gallegos	Pantano Dumestre	7	CAMS 129006	-51.8053	-72.4356	12895	45	15410.5	204.5
2011	Rio Gallegos	Eberhardt	7	CAMS 98831	-51.5779	-72.6684	13690	45	16534.5	233.5
2011	Rio Gallegos	Pantano A. Varas	7	CAMS 98832	-51.7589	-72.8112	9210	40	10374	122
2011	Rio Gallegos	Vega Benitez	7	CAMS 98916	-51.5582	-72.5828	12490	40	14678.5	352.5

2 Additional chronological discussion

The relationship between our reconstructed time steps and published chronological constraints is described in Section 6.2 of the main text. However, there are subtleties associated with much of this chronological information that benefit from a more detailed version of this discussion. In this section, we describe the dates available for each ice lobe during each of our reconstructed time steps, and provide the landform context from our reconstruction. It is worth noting that while the dates are from the published literature, we (re-)assign those dates to our eight time steps in this study.

2.1 Time step 1: Pre-global Last Glacial Maximum (gLGM) advance

The Río Gallegos lobe flowed rapidly to its greatest extent during time step 1, creating flowsets FS 1 and FS 2 (Figure 13A in the main text). The extent of the other ice lobes is unclear, but the Skyring lobe cannot have been fully extended because the geomorphology of the Río Gallegos and Skyring lobes overlaps and Skyring drainage later flowed into the former Río Gallegos depression. Cosmogenic ^{10}Be exposure ages of 56.0 ka and 138 ka from the outer limits of the Río Gallegos lobe are substantially younger than the Bella Vista flow, which has been ^{40}Ar/^{39}Ar dated to 1.17 Ma (Kaplan et al., 2007; Singer et al., 2004; Meglioli, 1992). The Bella Vista flow underlies till deposits thought to relate to the maximum glacial advance and the large difference in these ages may be due to post-depositional processes affecting moraine boulders sampled for exposure dating (Kaplan et al., 2007). We caution that linking distal drift sediments to limits defined by glacial geomorphology is challenging (e.g. Meglioli (1992) also dated flows to 8.0 and 8.5 Ma within this ice lobe); the Bella Vista flow only provides a maximum age for the limit; and it is not inconceivable that the ice lobe extended towards this maximum extent on several occasions.

2.2 Time step 2: Pre-gLGM advance

The Skyring, Otway, Magellan and BI-SSb ice lobes advanced to their maximum extents, whereas the Río Gallegos lobe retreated (Figure 13B in the main text). The Skyring lobe advanced into the Río Gallegos depression, overriding former moraines and glacial lineations to leave irregular dissected ridges (Section 4.2.3 in the main text). The precise extent and timing of the advances is unclear, and correlation cannot be made between the ice lobes. The ^{10}Be ages of 56.0 ka and 138 ka (Kaplan et al., 2007) in time step 1 could reasonably relate to time step 2 if they were actually deposited by the Skyring lobe. Two additional ^{10}Be ages of 59.4 ka and 173 ka from the Magellan lobe are similarly young compared to local ^{40}Ar/^{39}Ar ages (Meglioli, 1992; Singer et al., 2004; Kaplan et al., 2007). However, tying dated tills to glacial limits may not be straightforward. It is conceivable that the ice lobes advanced more than once to similar limits at radically different times, possibly due to topographic constraints (Kirkbride & Winkler, 2012; Barr & Lovell, 2014) or erosional feedbacks (Kaplan et al., 2009; Anderson et al., 2012). For example, The BI-SSb lobe was also close to this limit in at least time steps 3 and 4. The four cosmogenic dates available for time steps 1 and 2 may indicate two separate advances at around 173-138 ka and 59-56 ka, but the dates are not apparently in stratigraphic order. These dates also disagree with the conceptual age model for the region (Meglioli, 1992) and do not take into account erosion and/or exhumation processes (Kaplan et al., 2007).

2.3 Time step 3: Pre-gLGM advance

The Río Gallegos lobe continued to recede during time step 3 and the Skyring and Otway lobes retreated to close to the limits of their topographic basins (Figure 13C in the main text). The Magellan lobe may have re-advanced to form FS 11, although this flowset could equally have formed in time step 1 or 2. In the Río Gallegos lobe, two ^{10}Be ages of 56.3 ka and 56.6 ka and three ^{36}Cl ages of 38.1 ka to 55.2 ka are younger than expected (repeat samples; Evenson et al., 2009). However, four ^{10}Be ages of between 37.1 ka and 64.4 ka from interior lateral moraines may have been deposited at a similar time (Sagredo et al., 2011). There are no chronological constraints for the Skyring, Otway or Magellan lobes and correlation between the lobes cannot be made. The BI-SSb ice limit has been ^{10}Be dated (Kaplan et al., 2007, 2008), with twelve ages ranging from 15.2 ka to 57.3 ka, eight of which are within 26.8

ka and 33.0 ka. In addition, two ^{26}Al dates of 24.8 ka and 30.4 ka and four ^{36}Cl dates of 18.7 ka, 25.2 ka, 27.1 ka and 51.5 ka have been reported (Kaplan et al., 2007; Evenson et al., 2009). Post-depositional erosion and exhumation may have affected many of these boulder ages (Kaplan et al., 2007), so Darvill et al. (2015b) used a ^{10}Be/^{26}Al depth profile through outwash sediments to obtain an independent estimate of age for the BI-SSb lobe. This demonstrated that the limit was deposited during the last glacial cycle, possibly around 45.6 ka.

Numerous dating campaigns have yielded ages younger than previously thought, and a best estimate of age for time step 3 may be somewhere between 26.8 ka and 57.3 ka. The large spread of ages could result from post-depositional processes, possibly linked to gradual melt-out of the dead ice in hummocky terrain or boulder erosion (Kaplan et al., 2007; Schomacker, 2008; Darvill et al., 2015a). The latter could explain the offset between the dominant cluster of boulder ages between 27.0 ka and 36.2 ka, and the depth profile at 45.6 ka, in which case the depth profile would be a better estimate of the time of deposition.

2.4 Time step 4: Pre-gLGM advance

In time step 4, the Skyring and Otway lobes retreated to skirt the edges of their respective basins, with the Otway lobe possibly re-advancing to form FS 7 (Figure 13D in the main text). The Magellan lobe retreated to Primera Angostura and the Río Gallegos lobe continued to retreat, possibly re-advancing slightly to deposit FS 3. The BI-SSb lobe re-advanced close to the limit of time step 3, yielding two ^{10}Be dates of 24.3 ka and 224.1 ka (Kaplan et al., 2007). These dates are ambiguous, but a depth-profile through associated outwash yielded a more robust age of ca. 30.1 ka (Darvill et al., 2015b). Like time step 3, there is scatter in the boulder ages, perhaps due to post-depositional processes. For the Magellan lobe, four ^{10}Be ages between 24.8 ka and 36.9 ka and two ^{26}Al ages of 31.0 ka and 32.6 ka (Kaplan et al., 2007) imply that the limit may have been deposited at a similar time to that of the BI-SSb lobe. In addition, we suggest that four ^{10}Be dates of 27.4 ka to 29.9 ka on Península Juan Mazía, previously ascribed to a later advance (McCulloch et al., 2005b;

Kaplan et al., 2008), may have been deposited at this time given the similarity in ages. There are no ages for the Río Gallegos, Skyring or Otway lobes and it remains unclear to what extent these lobes acted in a similar manner.

2.5 Time step 5: Re-advances, rapid flow and lake drainage

The Río Gallegos, Magellan and Skyring lobes retreated during time step 5, with the latter triggering the development of a proglacial lake – palaeo-Laguna Blanca – which may have further facilitated ice loss from a calving front (Figure 13E in the main text). This lake drained northwards into the Río Gallegos depression, indicating recession of the Río Gallegos lobe. The Otway lobe re-advanced significantly, forming FS 8 around Laguna Cabeza del Mar and shifting the ice divide between the Otway and Magellan lobes south-eastward into the present-day Strait of Magellan. The BI-SSb lobe also re-advanced to a limit close to Bahía San Sebastián, depositing a large terminal moraine that is still preserved east of Laguna Larga and forming FS 17. The re-advances of these two ice lobes may have been in response to rapid ice flow, or possible surge-like activity. Thus, between time steps 4 and 5, all ice lobes receded and the Otway and BI-SSb lobes re-advanced. There are no chronological constraints for any of the ice lobes in this time step, but the moraines deposited by the Otway can be correlated with those of the Skyring and Magellan lobes.

2.6 Time step 6: Re-advances, rapid flow and lake drainage

All ice lobes retreated during this time step (Figure 13F in the main text). The Skyring, Otway and Magellan lobes did not retreat far because the potentially catastrophic drainage of palaeo-Laguna Blanca passed from in front of the Skyring lobe east to south-easterly in front of the Otway and Magellan lobes. It is unclear how far the Río Gallegos and BI-SSb lobes retreated during this time step, but the presence of deformed lacustrine sediments in re-advance moraines of the BI-SSb lobe in time step 7 suggests that this ice lobe must have retreated sufficiently for a pro-glacial lake to develop. Again, there are no chronological constraints for any of the ice lobes in this time step, but we note that for the Skyring, Otway and Magellan lobes, time steps 5 and 6 are broadly constrained by dates in the Magellan lobe for time steps 4 and 7, and that the limits can be correlated reasonably robustly across the three ice lobes. Dating the drainage of palaeo-Laguna Blanca would improve this chronology and test our interpretation of the dates for time steps 4 and 7.

2.7 Time step 7: The gLGM

This time step has previously been defined as the gLGM limit (Figure 13G in the main text). There are no supporting ages for the Río Gallegos, Skyring and Otway lobes, although they were likely situated within the present-day fjords, with the termini of the Skyring and Otway lobes splitting after time step 6. The Magellan and BI-SSb lobes had retreated – although it is not clear how far – and re-advanced during this time step, possibly displaying surge-like behaviour and forming FS 13 and FS 18. The Magellan lobe has been ^{10}Be dated four times on Península Juan Mazía to between 18.3 ka and 23.2 ka. The BI-SSb lobe has also been dated with 18 ^{10}Be dates yielding ages of between 15.6 ka and 55.8 ka, one ^{26}Al date of 26.6 ka, and two ^{36}Cl dates of 22.3 ka and 54.8 ka (McCulloch et al., 2005b; Kaplan et al., 2007, 2008; Evenson et al., 2009). Sixteen of the ^{10}Be dates fall between 17.6 ka and 24.9 ka. The reason for the scatter in ages is unclear, although the ^{10}Be date of 55.8 ka may be due to inheritance, given most of the dates are from a large erratic boulder train on the south-eastern side of Bahía Inútil (Darvill et al., 2015a). Nonetheless, the dates for the Magellan and BI-SSb lobes generally support the assertion that this time step relates to the gLGM.

2.8 Time step 8: Rapid retreat

All of the ice lobes were in full post-gLGM retreat during this time-step, likely developing proglacial lakes in front of their receding margins that could have increased the rate of ice retreat due to frontal calving (Figure 13H in the main text; Porter et al., 1992; Kilian et al., 2007). The Skyring and Otway lobes were located well within their respective fjords, with cores suggesting ice-free conditions in Seno Skyring and Seno Otway dated to at least 14.8 ka and 14.7 ka, respectively, using radiocarbon dating and tephrostratigraphy (Kilian et al., 2013). Kilian et al. (2007) suggested that this was part of a rapid retreat of the Skyring lobe, likely linked in part to proglacial calving. The Magellan lobe has been ^{10}Be dated to 20.4 ka and 20.6 ka on Península Juan Mazía and also 15.1 ka and 16.8 ka on the western lateral side of the lobe (Kaplan et al., 2008), perhaps indicating relatively rapid retreat of the ice lobe during and after this time step, and supporting ice recession by ca. 22 ka, as indicated by luminescence ages on the western side of the Strait of Magellan (Blomdin et al., 2012). The BI-SSb lobe has yielded five similar ^{10}Be dates between 18.7 ka and 21.3 ka (McCulloch et al., 2005b; Kaplan et al., 2008), as well as four ^{10}Be dates from below the proglacial lake shoreline suggesting that drainage may have occurred between 14.4 ka and 8.3 ka (Evenson et al., 2009). Numerous radiocarbon dates suggest that retreat of the Magellan and BI-SSb ice lobes was well under way by at least 14-15 ka (Clapperton et al., 1995; McCulloch & Bentley, 1998; McCulloch et al., 2005b), although the presence of the Reclús tephra within lake sediments suggests full retreat and lake drainage cannot have been before ca. 14.3 ka (McCulloch et al., 2005a). The rapid retreat, and possible collapse, of the BI-SSb lobe during and after this time step is supported by radiocarbon dates in the accumulation area of the lobe in central Cordillera Darwin that suggest that the constituent outlet glaciers that formed the ice lobe in this time step may have retreated into small interior fjords as early as 16.8 ka (Hall et al., 2013).

3 Supplementary references

Anderson, D.M. & Archer, R.B. (1999). Preliminary evidence of early deglaciation in southern Chile. *Palaeogeography Palaeoclimatology Palaeoecology* **146** (1-4), 295–301.

Anderson, R.S., Dühnforth, M., Colgan, W. & Anderson, L. (2012). Far-flung moraines: Exploring the feedback of glacial erosion on the evolution of glacier length. *Geomorphology* **179**, 269–285.

Balco, G., Stone, J.O., Lifton, N.A. & Dunai, T.J. (2008). A complete and easily accessible means of calculating surface exposure ages or erosion rates from 10Be and 26Al measurements. *Quaternary Geochronology* **3** (3), 174–195.

Barr, I.D. & Lovell, H. (2014). A review of topographic controls on moraine distribution. *Geomorphology* **226**, 44–64.

Blomdin, R., Murray, A., Thomsen, K.J., Buylaert, J.-P., Sohbati, R., Jansson, K.N. & Alexanderson, H. (2012). Timing of the deglaciation in southern Patagonia: Testing the applicability of K-Feldspar IRSL. *Quaternary Geochronology* **10** (0), 264–272.

Boex, J., Fogwill, C., Harrison, S., Glasser, N.F., Hein, A., Schnabel, C. & Xu, S. (2013). Rapid thinning of the late Pleistocene Patagonian Ice Sheet followed migration of the Southern Westerlies. *Sci. Rep.* **3**, 1–6.

Borchers, B., Marrero, S., Balco, G., Caffee, M., Goehring, B., Lifton, N., Nishiizumi, K., Phillips, F., Schaefer, J. & Stone, J. (2016). Geological calibration of spallation production rates in the CRONUS-Earth project. *Quaternary Geochronology* **31**, 188–198.

Clapperton, C.M., Sugden, D.E., Kaufman, D.S. & McCulloch, R.D. (1995). The Last Glaciation in Central Magellan Strait, southernmost Chile. *Quaternary Research* **44** (2), 133–148.

Darvill, C.M., Bentley, M.J. & Stokes, C.R. (2015a). Geomorphology and weathering characteristics of erratic boulder trains on Tierra del Fuego, southernmost South America: Implications for dating of glacial deposits. *Geomorphology* **228**, 382–397.

Darvill, C.M., Bentley, M.J., Stokes, C.R., Hein, A.S. & Rodés, Á. (2015b). Extensive MIS 3 glaciation in southernmost Patagonia revealed by cosmogenic nuclide dating of outwash sediments. *Earth and Planetary Science Letters* **429**, 157–169.

Evenson, E.B., Burkhart, P.A., Gosse, J.C., Baker, G.S., Jackofsky, D., Meglioli, A., Dalziel, I., Kraus, S., Alley, R.B. & Berti, C. (2009). Enigmatic boulder trains, supraglacial rock avalanches, and the origin of ‘Darwin’s boulders,’ Tierra del Fuego. *GSA Today* **19** (12), 4–10.

Hall, B.L., Porter, C.T., Denton, G.H., Lowell, T. V & Bromley, G.R.M. (2013). Extensive recession of Cordillera Darwin glaciers in southernmost South America during Heinrich Stadial 1. *Quaternary Science Reviews* **62** (0), 49–55.

Heusser, C.J. (1987). Fire history of Fuego-Patagonia. *Quaternary of South America and Antarctic Peninsula* **5**, 93–109.

Heusser, C.J., Heusser, L.E. & Hauser, A. (1990). A 12 000 yr BP Tephra layer at Bahía Inútil (Tierra del Fuego, Chile). *Anales del Instituto de la Patagonia* **19**, 39–49.

Kaplan, M.R., Coronato, A., Hulton, N.R.J., Rabassa, J.O., Kubik, P.W. & Freeman, S.P.H.T. (2007). Cosmogenic nuclide measurements in southernmost South America and implications for landscape change. *Geomorphology* **87** (4), 284–301.

Kaplan, M.R., Fogwill, C.J., Sugden, D.E., Hulton, N., Kubik, P.W. & Freeman, S.P.H.T. (2008). Southern Patagonian glacial chronology for the Last Glacial period and implications for Southern Ocean climate. *Quaternary Science Reviews* **27** (3-4), 284–294.

Kaplan, M.R., Hein, A.S., Hubbard, A. & Lax, S.M. (2009). Can glacial erosion limit the extent of glaciation? *Geomorphology* **103** (2), 172–179.

Kaplan, M.R., Strelin, J.A., Schaefer, J.M., Denton, G.H., Finkel, R.C., Schwartz, R., Putnam, A.E., Vandergoes, M.J., Goehring, B.M. & Travis, S.G. (2011). In-situ cosmogenic 10Be production rate at Lago Argentino, Patagonia: Implications for late-glacial climate chronology. *Earth and Planetary Science Letters* **309** (1-2), 21–32.

Kilian, R., Baeza, O., Ríos, F., Arz, H., Lamy, F., Witrz, J. & Baque, J. (2013). Evolución paleogeográfica y palaeoecológica del Sistema de fiordos del Seno Skyring y Seno Otway en la región de Magallanes durante el tardiglacial y Holoceno. *Anales del Instituto de la Patagonia*. [Online]. 41 (2) p.5–26.

Kilian, R., Schneider, C., Koch, J., Fesq-Martin, M., Biester, H., Casassa, G., Arévalo, M., Wendt, G., Baeza, O. & Behrmann, J. (2007). Palaeoecological constraints on late Glacial and Holocene ice retreat in the Southern Andes (53°S). *Global and Planetary Change* **59** (1–4), 49–66.

Kirkbride, M.P. & Winkler, S. (2012). Correlation of Late Quaternary moraines: impact of climate variability, glacier response, and chronological resolution. *Quaternary Science Reviews* **46** (0), 1–29.

Lal, D. (1991). Cosmic ray labeling of erosion surfaces: in situ nuclide production rates and erosion models. *Earth and Planetary Science Letters* **104** (2–4), 424–439.

McCulloch, R.D. & Bentley, M.J. (1998). Late glacial ice advances in the Strait of Magellan, southern Chile. *Quaternary Science Reviews* **17** (8), 775–787.

McCulloch, R.D., Bentley, M.J., Tipping, R.M. & Clapperton, C.M. (2005a). Evidence for late-glacial ice dammed lakes in the central Strait of Magellan and Bahia Inutil, southernmost South America. *Geografiska Annaler Series a-Physical Geography* **87A** (2), 335–362.

McCulloch, R.D. & Davies, S.J. (2001). Late-glacial and Holocene palaeoenvironmental change in the central Strait of Magellan, southern Patagonia. *Palaeogeography Palaeoclimatology Palaeoecology* **173** (3-4), 143–173.

McCulloch, R.D., Fogwill, C.J., Sugden, D.E., Bentley, M.J. & Kubik, P.W. (2005b). Chronology of the last glaciation in central Strait of Magellan and Bahia Inutil, southernmost South America. *Geografiska Annaler Series a-Physical Geography* **87A** (2), 289–312.

Meglioli, A. (1992). *Glacial Geology and Chronology of southernmost Patagonia and Tierra del Fuego, Argentina and Chile*. Lehigh.

Porter, S., Clapperton, C. & Sugden, D. (1992). Chronology and dynamics of deglaciation along and near the Strait of Magellan, southernmost South America. *SGU series Ca. Research paper*

Porter, S.C. (1990). Character and ages of Pleistocene Drifts in a transect across the Strait of Magellan. *Quaternary of South America and Antarctica Peninsula* **7**, 35–49.

Putnam, A.E., Schaefer, J.M., Barrell, D.J.A., Vandergoes, M., Denton, G.H., Kaplan, M.R., Finkel, R.C., Schwartz, R., Goehring, B.M. & Kelley, S.E. (2010). In situ cosmogenic 10Be production-rate calibration from the Southern Alps, New Zealand. *Quaternary Geochronology* **5** (4), 392–409.

Reimer, P. (2013). IntCal13 and Marine13 Radiocarbon Age Calibration Curves 0–50,000 Years cal BP. *Radiocarbon* **55** (4), 1869–1887.

Sagredo, E.A., Moreno, P.I., Villa-Martinez, R., Kaplan, M.R., Kubik, P.W. & Stern, C.R. (2011). Fluctuations of the Última Esperanza ice lobe (52°S), Chilean Patagonia, during the last glacial maximum and termination 1. *Geomorphology* **125** (1), 92–108.

Schomacker, A. (2008). What controls dead-ice melting under different climate conditions? A discussion. *Earth-Science Reviews* **90** (3–4), 103–113.

Singer, B.S., Ackert, R.P. & Guillou, H. (2004). 40Ar/39Ar and K-Ar chronology of Pleistocene glaciations in Patagonia. *Geological Society of America Bulletin* **116** (3-4), 434–450.

Stern, C.R. (1992). Tefrocronologia de Magallanes: nuevos datos e implicaciones. *Anales del Instituto de la Patagonia* **21**, 129–141.

Stone, J.O. (2000). Air pressure and cosmogenic isotope production. *J. Geophys. Res.* **105**

(B10), 23753–23759.

Stuiver, M., Reimer, P.J. & Reimer, R.W. (2005). *CALIB 5.0*. 2005. http://calib.qub.ac.uk/calib/.

Uribe, P. (982). Deglaciacion en el sector central del Estrecho de Magallanes: consideraciones geomorfologicos y cronologica. *Anales del Instituto de la Patagonia* **13**, 103–111.